# Water Droplet Calibration of a Cloud Droplet Probe and In-Flight Performance onboard the NOAA WP-3D in Liquid, Ice and Mixed-Phase Clouds during ARCPAC

Sara Lance[1,2] and Charles A Brock[1]
[1]Chemical Sciences Division, National Oceanic and Atmospheric Administration
[2]Cooperative Institute for Research in Environmental Sciences

Dave Rogers[3]
[3]National Center for Atmospheric Research

Joshua A. Gordon[4]
[4]National Institute of Standards and Technology

## Abstract

Laboratory calibrations of the CDP sample area and droplet sizing are performed using water droplets of known size, generated at a known rate. Following calibration, the sizing bias is shown to be less than 15% and the sample area is determined to within 10% for 12 um and 22 um diameter droplets. However, comparison with an independent measure of liquid water content (LWC) during in-flight operation suggests much greater biases in the droplet size and/or droplet concentration measured by the CDP. Since the bias in CDP-LWC is strongly concentration dependent, we hypothesize that this discrepancy is a result of coincidence, when two or more droplets pass through the CDP laser beam within a very short time. The coincidence error, most frequently resulting from the passage of one droplet outside and one inside the instrument sample area at the same time, is evaluated in terms of an "extended sample area" ($SA_E$), the area in which individual droplets can affect the sizing detector without necessarily registering on the qualifier. $SA_E$ is calibrated using standardized water droplets, and used in a Monte-Carlo simulation to estimate the effect of coincidence on the measured droplet size

distributions. The simulations show that extended coincidence errors are important for the CDP at droplet concentrations even as low as 200 $cm^{-3}$, and these errors are necessary to explain the trend between calculated and measured LWC observed in liquid and mixed-phase clouds during the Aerosol, Radiation and Cloud Processes Affecting Arctic Climate (ARCPAC) study. We estimate from the simulations that 60% oversizing error and 50% undercounting error can occur at droplet concentrations exceeding 500 $cm^{-3}$. Modification of the optical design of the CDP is currently being explored in an effort to reduce this coincidence bias.

## 1. Introduction

### *1.1 Measurement of Cloud Particles*

There are limitations to every cloud measurement technique. The wide range of cloud particle sizes (~1 um to 10 mm in diameter) and number concentrations (~$10^{-5}$ to $10^3$ $cm^{-3}$) that naturally exist very often necessitates more than one measurement technique or a suite of instruments that are each tuned to specifically detect a subset of the cloud particle population. Quantitative measurement of ice clouds and mixed-phase clouds can be particularly challenging for both remote-sensing and in situ measurement techniques. However, even for non-precipitating liquid-only clouds, measurement interpretation requires a great deal of caution. In situ measurements of individual cloud droplets using optical methods can be subject to a wide variety of instrument biases and limitations, which are the focus of this paper.

Uncertainties in droplet counting and sizing together result in greater uncertainty for higher order products such as liquid water content (LWC, the mass of liquid water in a given volume of air) calculated from the observed cloud droplet size distributions. Comparison to independent observations of LWC, using a measurement technique characterized by different intrinsic uncertainties, is therefore a useful method for testing the accuracy of droplet size distribution measurements; to accurately calculate LWC, the droplet size distribution must be known even more accurately since LWC is proportional to the third power of droplet size. Another specific challenge for in situ cloud droplet measurements using optical methods is the definition of a sample volume. The cross-sectional area in which droplets are detected, defined by the optical and electronic configuration of the instrument, when multiplied by the flow velocity (normal to the sample area) and the sample duration, yields the sample volume. A bias in the sample area or in the flow velocity translates directly to a bias in measured droplet concentrations and calculated LWC. Hereafter, we refer mainly to the sample area rather than the sample volume, since the focus of the paper is on the cloud probe performance.

Although multiple cloud measurements can be used to complement each other using optimal estimation methods [Feingold, et al 2006], it is often difficult to find a fair basis for comparison between different remote-sensing and in situ cloud observations, and ultimately to use either to validate the other, due to the multiple degrees of freedom between the parameters each measures best. The lack of an objective standard makes the validation of in situ droplet measurements a challenging task, one that is not addressed the same way by all researchers. Often, redundant in situ instruments, covering the same cloud particle size range and operating from the same sampling platform, are used to address this problem. However, it is not always possible to reconcile observational differences between the various in situ measurements, which can be quite significant [e.g.

McFarquahar et al, 2007; Baumgardner, 1983]. Laboratory calibrations are performed to resolve these differences, with the ultimate purpose of distinguishing natural ambient variability from measurement uncertainty.

The sizing performance of in situ cloud probe instruments is typically calibrated in the laboratory by injecting standardized particles directly into the sample area of the open path laser beam. The type of calibration particles used, most often glass beads or polystyrene latex (PSL) spheres, have their own unique response in the instrument. For most in situ cloud droplet measurements, following calibration with standardized particles, the response of the instrument to water droplets must be calculated with assumptions about the laser and downstream optics because of the difference in refractive index between water and the calibration particles. To avoid these assumptions, calibration with water droplets is preferred since ambient cloud droplets are typically dilute aqueous solutions, which are expected to behave optically like pure water droplets [Diehl et al, 2008]. Generation of a standardized droplet size and number concentration of water droplets for calibration is not a trivial task. Despite the difficulty, however, it has been shown that such an effort is worthwhile. For instance the forward scattering spectrometer probe (FSSP) was shown to oversize water droplets of 15-30 um diameter by up to 15% when using glass beads for calibration [Wendisch et al, 1996], which then leads to as much as a 52% overestimate in LWC even when the droplet concentration is measured with 100% accuracy.

An important characteristic of droplet generation methods employed by, e.g. Nagel et al [2007], Wendisch et al [1996], Korolev et al [1985; 1991], Jonnson and Vonnegut [1982], and Schneider and Hendricks [1964], is the steady production of droplets one-at-a-time in the laboratory greatly reducing any possibility of coincidence errors, which occur when two or more droplets pass through the sample area at the same time. The droplet generation method employed by Nagel et al [2007] to evaluate the FSSP utilizes a commercial piezo-electric ink-jet device. Taking advantage of the steady production rate of calibration droplets, it is possible to test the counting efficiency of the cloud probe instrument and to clearly map the sample area.

In the end, however, even this type of carefully crafted laboratory calibration is not fully representative of in situ measurements, as artifacts can arise solely during in-flight operation. It is well known, for instance, that the external geometry of a cloud probe instrument can significantly alter the measured cloud particle size distribution as a result of large droplets and ice crystals shattering upon impact with parts of the instrument that extend upstream of the sample volume [Heymsfield, 2007; McFarquahar et al, 2007; Korolev and Isaac, 2005]. Wind-tunnel studies can be used to simulate the in-flight environment to evaluate potential problems such as those related to cloud particle shattering, changes to the cloud particle trajectory, or icing of the cloud probe. However, these types of artifacts are difficult to quantify in a laboratory setting due in large part to the difficulty of continuously generating and uniformly transmitting ice crystals with realistic sizes, shapes and concentrations at high velocities upstream of a cloud droplet probe.

In situ LWC measurements from hot-wire probes provide an independent observation for validating measured cloud droplet size distributions from a single aircraft sampling platform. However, hot-wire measurements have their own limitations; e.g. 1) they are limited to non-precipitating conditions, as their sensitivity declines appreciably and unpredictably for droplet sizes above ~40 um due to droplet splattering [Biter et al, 1987; Feind et al, 2000], 2) the collection of small droplets (< 5 um) is also less than 100% efficient [King et al, 1978], and 3) a percentage of the ice present in ice-only or mixed-phase clouds mass may be mistakenly attributed to liquid water. Thus, while hot-wire LWC measurements and optical cloud probe measurements are complementary to one another and should be flown together whenever possible, careful and detailed laboratory calibrations with water droplets are also necessary for fundamental evaluation of a cloud droplet probe.

In this study we use standardized water droplets generated in the laboratory to quantify the uncertainties of one in situ cloud probe instrument, the CDP, manufactured by Droplet Measurement Technologies, Inc (mention of this product is not an endorsement but only serves to clarify the hardware that was used). A further goal of this study is to evaluate the performance of the CDP during airborne operation onboard the NOAA WP-3D during the Aerosol, Radiation, and Cloud Processes affecting Arctic Climate (ARCPAC, http://www.esrl.noaa.gov/csd/arcpac/) project, which took place in the Alaskan Arctic in April 2008, by comparing the measured droplet size distributions with hot-wire LWC measurements. CDP observations in liquid, ice and mixed-phase clouds sampled during ARCPAC are discussed.

### *1.2 ARCPAC*

The ARCPAC field campaign was designed to evaluate the climatic effects of Arctic Haze [Brock et al, *in preparation*], including the indirect effects of aerosols on Arctic clouds. Low level clouds in the Arctic springtime can warm the surface by absorbing in the infrared [Curry and Ebert, 1992; Curry et al, 1993]. It is expected that changes in the concentrations of either cloud condensation nuclei or ice nuclei can affect the drop size distribution and even the cloud phase, thereby changing cloud radiative properties [Lubin and Vogelmann, 2006; Garrett and Zhao, 2006]. Also of interest is the removal of particles by clouds, especially as deposition of soot and other absorbing aerosols onto snow surfaces can significantly alter the surface albedo [McConnell et al, 2007]. In recent years, special interest in both of these processes has been fueled by faster-than-expected warming in the Arctic and an accelerated rate of Arctic sea-ice melt [Alekseev et al, 2009; Serreze and Francis, 2006]. For our ultimate goal of understanding the aerosol-cloud-interactions in the Arctic, we first evaluate the uncertainties and limitations of the CDP observations obtained during ARCPAC.

## 2. Methods

### *2.1 Overview of the Instrumentation*

Table 1 lists instruments relevant for in situ cloud sampling onboard the NOAA WP3-D during the ARCPAC campaign.

| Instrument Name | Acronym | Method | Range | units |
|---|---|---|---|---|
| Cloud and Aerosol Spectrometer<br>Serial #: CAS-0708-017 | CAS | Forward / Back Optical Scattering | 0.6 – 50 | um |
| Cloud Droplet Probe<br>Serial #: CCP-0703-010 | CDP | Forward Scattering | 3 – 50 | um |
| Cloud Imaging Probe<br>Serial #: CCP-0703-010 | CIP | 2D image | 25 – 2000 | um |
| Precipitation Imaging Probe<br>Serial #: PIP-0705-005 | PIP | 2D image | 100 – 6000 | um |
| CSIRO King Probe | King-LWC | Hot-wire | 0.1 – 6.0 | g $m^{-3}$ |

| | | | | |
|---|---|---|---|---|
| Johnson-Williams Probe | JW-LWC | Hot-wire | 0.1 – 6.0 | g $m^{-3}$ |

During ARCPAC, the in situ cloud probes were mounted below and forward of the port-side wing tip of the NOAA WP-3D, while the LWC probes were mounted along the lower side of the fuselage, well forward of the port-side wing.

The CSIRO King-LWC measurements are an important part of this study, for evaluating the in-flight performance of the CDP. These measurements are corrected by first determining the signal offset in clear-air as a function of the ambient temperature, pressure and true air speed measurements [King et al, 1978; King et al, 1981; King et al, 1985], where clear-air is identified from the cloud probe measurements. We do not manually correct for baseline drift, as some researchers do, by subtracting a bias determined from linear interpolation between measurements before and after each cloud penetration, thereby forcing the clear-air LWC measurements to zero, due to the subjective nature of the procedure. We evaluate the accuracy of the corrected King-LWC measurements by comparing vertical profiles of measured LWC to the expected adiabatic profiles for low altitude stratus with a given cloud base temperature and pressure. The King-LWC measurements often approach the adiabatic condition but are never super adiabatic, which gives us confidence in the physicality of the measurements. For our analysis, we do not use King-LWC measurements for LWC values below 0.1 g $m^{-3}$ due to uncertainties caused by baseline drift and temporary hysteresis following sustained liquid or ice impaction. This detection limit of 0.1 g $m^{-3}$ is conservative, as the baseline drift for the King-LWC measurements was almost always below 0.02 g $m^{-3}$. The JW-LWC probe on the WP-3D aircraft, although reportedly more precise, was found to be much less reliable than the King-LWC probe during ARCPAC; the baseline for the JW-LWC measurements drifted by as much as 0.2 g $m^{-3}$ (though more typically by 0.05 g $m^{-3}$) throughout the campaign without any apparent systematic cause. The JW-LWC measurements are therefore not used.

Both the CIP and PIP produce images of individual particles by the shadows they cast on a photodiode array as they transit across a laser beam, in a manner similar to the optical array probes used by Korolev et al [1991]. The uncertainties of these instruments are outside the scope of this paper, and the uncorrected particle size distributions and images are used to provide a context for the ambient conditions encountered.

The CAS and the CDP are single-particle instruments that measure the light scattered from a droplet or large particle passing through an open path laser beam. Both the CAS and CDP make use of two photodetectors to constrain the optical sample area. Although the CAS measurement covers a range of sizes that includes the size range of the CDP, we do not report observations from the CAS in this paper. The CAS has been successfully applied in cloud droplet closure studies previously (Fountoukis et al [2007]; Meskhidze et al [2005]; Conant et al [2004]), however, the performance of the CAS used in ARCPAC has not been documented, and preliminary analysis indicates some problems with the measurements, which need to be addressed separately.

While the performance of other single particle forward scattering probes like the FSSP have been documented in detail in many studies [e.g. Baumgardner et al, 1985; Baumgardner and Spowart, 1990; Brenguier et al, 1998; Wendisch et al, 1996; Nagel et al, 2007], the CDP differs in terms of its optics, electronics and external geometry. Specific aspects regarding the expected performance of the CDP are outlined in the following sections.

*2.2 CDP Sample Area*

The optical cross section of the laser beam path for which particles are deemed in-focus, or qualified sample area ($SA_Q$), is a necessary parameter for quantifying the ambient particle number concentration. This cross-sectional area, when multiplied by the sampling time and the flow velocity perpendicular to the sample area plane, yields the sample volume; thus, uncertainties in the sample area translate directly to uncertainties in particle concentrations. Calibration of sample area has been performed previously for the FSSP using a spinning disk with a wire attached [Nagel et al, 2007] and a pinhole [Brenguier et al, 1998] with fine positioning control. However, calibration of the CDP sample area has not been previously published, nor have researchers consistently reported the value used for the sample area in calculating droplet concentrations from CDP data.

Particles are considered within the sample area when they lie within the depth of field (DoF) of the optics and are therefore in-focus. These qualified particles are a subset of all detected particles. The CDP qualifies a detected particle as either within or outside $SA_Q$ with the use of an unmasked photodetector (sizer), a masked photodetector (qualifier) and a comparator circuit. Light scattered by a particle is collected over a range of angles ~4-12$^{o}$ in the forward direction and then split between the qualifier and sizer. When the qualifier voltage is larger than the sizer voltage, the particle is considered inside the DoF and is therefore counted. The amplitude of the sizer pulse is then used to determine the size of the droplets within $SA_Q$, as discussed in the next section.

The qualifier mask of the CDP is a rectangular slit configuration, with long side parallel to the air flow, which is fundamentally different from the optical mask of the original FSSP "annulus" detector (used to qualify whether particles are in the DoF), which has a masked central region that is circular in shape. However, both utilize the same basic principle; when the droplet image is out-of-focus, the image is larger and more diffuse [Burnet and Brenguier, 2002], allowing more or less light to reach the detector, depending on the optical configuration. The original FSSP annulus detector measures a low voltage when the droplet is in-focus (because the in-focus image is almost entirely masked), whereas the CDP qualifier measures a low voltage when the droplet is out-of-focus (because the out-of-focus image is larger than the slit in the qualifier mask, and therefore only a fraction of the total scattered light is detected). The newer FSSP models (e.g. Fast-FSSP and FSSP-300) use an optical mask with a similar shape to the slit in the CDP [Burnet and Brenguier, 2002]. The slit configuration limits droplet detection to positions along the centerline of the laser beam where laser intensity is more homogeneous.

*2.3 CDP Droplet Sizing*

The amount of light diffracted by a droplet is proportional to the square of the droplet size and also depends on the laser wavelength, and scattering angle. For the droplet size range of the CDP and the wavelength of the CDP laser, this relationship is expected to follow Mie theory [Bohren and Huffman, 1983]. The light collected over a given range of scattering angles (e.g. ~4-12$^o$ in the CDP) can then be related to a droplet size by assuming that the droplets have a refractive index equal to that of pure water.

To calibrate the sizing photodetector response to a given droplet size, particles are injected into the sample area of the CDP. If glass beads or polystyrene latex spheres are used to calibrate the CDP sizer, the response of the CDP to water droplets must be calculated based on the difference in refractive index between water and glass, for instance. The scattering collection angles of the photodetector must be known accurately to apply this technique. Calibrating the CDP with water droplets avoids this uncertainty.

### *2.4 Sources of Uncertainty for the CDP*

The potential sources of error for in situ cloud probe observations result from different mechanisms ranging from optical, electronic, statistical and physical in nature. We briefly outline many of these different sources of error for the CDP, which have previously been identified in the evaluation of other forward scattering probes. Brenguier et al [1998] cover many of these issues in detail.

1) Size Resolution Limits due to Mie Resonance

Droplet sizing by the CDP is limited by discrete binning of measured pulse heights, with a default of 30 bins covering the range from 3-50 um. The bins prescribed by the manufacturer are 1 um wide from 3 to 14 um, after which they become 2 um wide. Although the bin definitions can be changed in the instrument software, the sizing of the CDP is expected to be fundamentally constrained by the non-monotonic relationship between droplet size and scattered light signal. Mie resonance structure is most pronounced for a single mode laser such as used in the CDP, while a multi-mode laser, as is used in the standard FSSP, dampens the Mie resonances [Knollenberg et al, 1976]. However, the single-mode CDP diode laser (658 nm) avoids the greater spatial intensity inhomogeneity of a multi-mode laser, which results in a greater broadening of the measured droplet size distribution [Baumgardner et al,1990] in addition to a shift in the measured mean size [Hovenac and Lock, 1993].

2) Electronic Response Time

Electronic response time can be an important limitation, both for counting all the droplets [Baumgardner et al, 1985] and for sizing them correctly [Baumgardner and Spowart, 1990]. The CDP has very small deadtime losses, and uses a 40 MHz clock. Faster electronics is one of the major improvements of the CDP over its predecessors.

3) Coincidence

Coincidence, which occurs when two or more droplets transit the sample area at the same time, is a concentration dependent problem that can cause undercounting and/or oversizing errors, and in general broadens the droplet size distribution. There are at least two types of coincidence in open path optical particle counting instruments, which have been previously discussed by Baumgardner et al [1985] and Cooper [1988]. The first type of coincidence, standard coincidence, occurs when two droplets pass through the qualified sample area, $SA_Q$, within rapid succession so that only one droplet is counted, and the size of the droplet appears to be larger than either of the single droplets alone because additional laser light is scattered into the sizing detector. The probability of standard coincidence occurring in the CDP onboard the NOAA WP-3D aircraft is less than 5% at droplet concentrations of 500 $cm^{-3}$, since the sample volume of the CDP at 1Hz is only ~0.06 $mm^3$ at an aircraft speed of 100 m $s^{-1}$.

Another type of coincidence can occur, with one droplet passing through $SA_Q$ and another droplet passing simultaneously just outside of $SA_Q$ but in an area where scattered light can still be detected. We refer to this region where non-qualified droplets may contribute scattered light to the signal from qualified droplets as the extended sample area, $SA_E$, and this type of coincidence as extended coincidence. When extended coincidence occurs, two things may happen: 1) the droplet passing through $SA_Q$ will be counted but may be oversized due to additional light scattered into the sizing detector from non-qualified droplets, or 2) the droplet passing through $SA_Q$ will not be counted because the additional light scattered from the coincident droplet can raise the sizer signal above the qualifier signal.

Typically, coincidence errors in existing cloud droplet instruments are considered minor for droplet concentrations less than 500 $cm^{-3}$ [Baumgardner et al, 1985]. Cooper [1988], Brenguier et al [1998] and Burnet and Brenguier [2002] present methodologies for correcting FSSP and Fast-FSSP measurements for coincidence errors, but conclude that correcting for coincidence errors on the shape of the droplet size distribution is both computationally expensive and ill-conditioned, due to a lack of constraints on the actual droplet spectrum.

4) Counting Statistics

Statistical uncertainties result from the finite sample volume. With a 1 Hz sampling rate, on an aircraft such as the NOAA WP-3D flying at 100 m $s^{-1}$, spatial variability within clouds cannot be resolved for spatial scales smaller than 100 m. The random statistical uncertainty in concentration is determined by Poisson statistics based on the number of droplets measured in a sampling period. The uncertainty in droplet concentration due to counting statistics is less than 5% for measured droplet concentrations above 13 $cm^{-3}$ (given a 1 Hz sampling rate, aircraft velocity of 100 $m\ s^{-1}$, and qualified sample area of 0.3 $mm^2$).

5) Particle Shattering

In situ cloud probe measurements have had issues with shattering of large particles, both liquid and ice, upstream of the laser detector [Jensen et al, 2009; McFarquahar et al, 2007; Field et al, 2006; Korolev and Isaac, 2005] either by direct impaction by the instrument arms or by the shear forces as the particles are deflected by the airstream flowing around the probe. Particle shattering typically results in an instrument bias towards smaller and more droplets. Unfortunately, correcting for artifacts resulting from particle shattering is often not feasible, as the magnitude of the error can be strongly sensitive to the many different factors including instrument geometries, aircraft attack angles and speed, as well as the particle size distribution, ambient temperature and the physical shape of the ice crystals. One potentially important advantage of the CDP compared to the FSSP is the use of two aerodynamic arms upstream of the open optical path, rather than the cylindrical inlet of the FSSP or CAS (which can be subject to large particle shattering artifacts [Heymsfield, 2007]). McFarquhar et al [2007] assert that the original CDP with rounded tips suffers much less from shattering artifacts than does the CAS. The sharply pointed asymmetric tips on the CDP used during ARCPAC (Figure 1a) are expected to further reduce shattering artifacts, especially in ice and in mixed-phase and precipitating clouds.

The interarrival time, or the time between observations of individual particles, gives a diagnostic of the extent of particle shatter on the particle size distribution, but significant uncertainty remains even after removing from the analysis those particles which are detected in groups of short interarrival times [Alexei Korolev, *in preparation*]. The CDP used during ARCPAC did not record particle interarrival times.

6) Particle Velocity

During in-flight operation, uncertainty in the particle velocity as it crosses the laser path also translates directly and proportionally to uncertainty in the droplet concentration, because the velocity in part defines the sample volume. During ARCPAC, the cloud probes were suspended beneath (and slightly in front of) the outboard wing tip of the NOAA WP-3D to minimize effects from the wake of the aircraft. However, measurements made at three different points on the aircraft all show different values for true air speed (TAS), with a -12 m $s^{-1}$ and -18 m $s^{-1}$ bias in the readings of the CIP and CAS pitot tubes, respectively, compared to the aircraft TAS. The CIP pitot tube is closest in proximity to the CDP. To be conservative, we assume that the bias between TAS calculated from different sensors is due to measurement bias rather than real differences in airflow at the different locations. We use the aircraft TAS in calculations of droplet concentration, both because we expect it to be the most accurate measurement and because the small pitot tubes located in close proximity to the probes, although heated, often became blocked with ice during flights in the Arctic. Since the aircraft TAS is the highest of the three TAS readings, we report the lowest expected droplet concentrations.

Therefore, we assume an uncertainty in TAS of 18 m $s^{-1}$, which results in an uncertainty in droplet concentrations of ~ 20%.

*2.4 Calibration System*

A calibration system was developed to quantify uncertainties relating to the CDP sample area, sizing resolution, coincidence errors and electronic response time using monodisperse water droplets 8-35 µm in diameter. Table 2 lists the main components of the calibration system, with many similarities to the systems used by Wendisch et al [1996] and Nagel et al [2007]. Lee [2003] provides a comprehensive description of droplet generation methods.

| **Component Description** | **Manufacturer/ Supplier** | **Model #/ Part #** | **Specifications** |
|---|---|---|---|
| Metrology camera w/ high speed shutter | JAI | CV-A10 CL | 0.5” CCD<br>1/60 - 1/300,000 $s^{-1}$ shutter speeds<br>0.44 MPixel resolution (575 x 760 pixels) |
| Diagnostic camera | BigCatch USB digital cameras | EM-310C | 0.5” CMOS |
| Microscope objectives and lens tubes | Edmund Optics | - | 4x, 10x and 20x magnifications |
| Drop generator device/ Piezo-electric actuator | MicroFab, Inc. | MJ-ABP-30/ JetDrive III | 30 um orifice/ Strobe control |
| Evaporation flow-tube | Allen Scientific Glass | - | 11” long evaporation section, ID = 2 cm, tapering to nozzle with ID = 0.5 mm |
| Oscilloscope | Tektronix | THS720A | 2 channel<br>100 MHz |
| Water pump | McMaster-Carr | 8220K43 | low flow gear pump |
| Water manifold | Cole-Parmer | A-06464-85 | (4) 3-way valves |
| Image acquisition card | National Instruments | PCIe-1427 | - |

Droplets were generated using a commercial piezoelectric drop generator. Stable operation of the generator (production of a single, straight jet of uniform droplets, without production of smaller satellite drops), requires specific operating parameters, which are fluid and orifice dependent. For generation of water droplets using a 30 um nozzle, the most stable operation is maintained with the following parameters: 3 us rise, 22 us dwell, 3 us fall, 44 us echo, 3 us final rise, 0 volts idle, 16 volts dwell and -16 volts echo at 250 Hz. These parameters produce ~40 um droplets. A 2 um nylon filter is used in the liquid flow upstream of the droplet dispensing device. Care must be taken to eliminate bubbles from the water supply to the device. The droplet generation system uses a liquid pump and a manifold of valves to allow transitioning between three different modes of operation without allowing bubbles into the system. These three modes of operation are: 1) purging the drop generator device using a liquid pump with a positive pressure head, 2) drawing in a cleansing solution via a negative pressure head, and 3) operating the drop generator device under static pressure in equilibrium with a water reservoir, bypassing the liquid pump altogether (normal operation). Periodic wetting and purging of the device eliminates bubbles and also prevents accumulation of electric charge on the outer surface of the glass nozzle, which can alter the droplet trajectories and prevent droplet generation. It was discovered that droplet generation was not as sensitive to the water reservoir pressure head as expected from previous studies (e.g. Wendisch et al [1996]) as long as the level of the water reservoir was below the tip of the drop generation device, resulting in a slight negative pressure and a concave meniscus. Vertical operation is also important, as a symmetrical meniscus in the droplet dispensing device nozzle prevents the droplet jet from ejecting at an angle, or from not being generated at all. Thus, the CDP is oriented vertically during the calibrations. The performance of the drop generator device is monitored with a diagnostic camera at 4x magnification and an LED strobe light synchronized to the piezo-electric actuator signal with a variable delay control, similar to Schafer et al. [2007].

Generated droplets then pass through an evaporation flow-tube (Fig. 1b) to accelerate the drops to greater speeds and to make fine adjustments to the droplet size by controlled evaporation. The droplets are injected into a laminar, dry sheath air. The residence time between the point of injection and the exit of the flow-tube controls the extent of droplet evaporation. The residence time can be controlled by changing either the sheath flow rate or the injection position of droplets inside the flow-tube. The speed of the droplets exiting the flow-tube is sensitive to both the flow rate and the droplet size; large droplets require a finite travel distance for acceleration, which is a function of the particle relaxation time. By varying the injection position and the flow rate, it is possible to explore two different effects (droplet size and speed) on the sizing and counting efficiency of the CDP. Water and piezo-electric actuator pulses are supplied within the injection positioning rod. A residence time of several seconds is required to evaporate droplets from 40 um to less than 10 um, depending on the relative humidity (RH) in the flow-tube. Neither the RH nor the residence time of droplets in the flow-tube was monitored; instead the droplet size was determined with an independent measurement, as explained below. The droplets accelerate to velocities up to 45 m $s^{-1}$ in the tapered section of the flow-tube. Figure 1a shows a photograph of the evaporation flow-tube during calibration of the CDP. The exit of the flow-tube nozzle was positioned less than 5 mm above the CDP sample area.

For independent verification of the droplet diameter, we utilize the "glares technique" described in previous papers [Korolev et al, 1991; Wendisch et al, 1996; Nagel et al, 2007], in which a camera directly images droplets as they pass through the laser beam of the CDP. The geometry of specular reflections off the front and back face of droplets, as observed by a camera situated at a given angle from the incident light, uniquely constrains the droplet size. The top image in Figure 1a shows a single droplet illuminated by the CDP laser beam, with two bright "glares" produced at the edge of the droplet image. Although the image is vertically blurred slightly due to the droplet motion, the shape of the droplet is apparent by way of independent backlighting (used for acquisition of this image only). Linear glares are produced when the droplet transits across a passive camera, allowing the glares to streak across the acquired image [e.g. Nagel et al, 2007]. The distance between the centerlines of the two glare streaks is $D_{glares}$. At a viewing angle of $130^o$ $D_{glares}$ is least sensitive to viewing angle, and the true droplet diameter, $D_{true}$, is ~10% greater than $D_{glares}$ [Wendisch et al, 1996]. Since the light source for the glares measurement is the CDP laser, this technique allows for verification of the droplet size within the sample area of the CDP, simultaneous to, but not affecting, the standard CDP measurement. For measuring $D_{glares}$, we use a digital metrology camera at 20x magnification focused on droplets as they transit the sample area of the CDP, with a viewing angle of $130^o$ to the incident light. The positioning of the droplets is highly repeatable as verified by observing that droplets remain in-focus and consistently positioned in the acquired image during the calibration experiments. The sizing of the metrology camera is independently calibrated both with backlit glass beads adhered to a transparent slide and with a standard optical test target. The uncertainty in the droplet sizing is dominated by the pixel resolution of the metrology camera setup, which is 0.54 um/pixel. Uncertainty in droplet positioning is ~10 um.

The droplet velocity is quantified by measuring the length of the droplet glares (parallel to the droplet trajectory and perpendicular to $D_{glares}$) while varying the amount of time the shutter of the metrology camera is held open. The slope of this relationship provides the droplet velocity. The maximum droplet velocity measurable is dependent on many factors including the optical magnification, the field of view, the pixel size resolution, the amount of light scattered and collected, the width of the laser beam, and the maximum shutter speeds available. 10x magnification was found to produce the optimum conditions for measuring the velocity of 10-20um droplets, which allows for a maximum droplet velocity measurement of ~70 m $s^{-1}$ across the CDP laser beam. For smaller droplets, the maximum measureable droplet velocity is lower, due to the dimness of the glares.

Droplet velocity may be important for several different reasons: 1) the electronic response time of the CDP may truncate the pulses when droplets pass at a faster velocity [Baumgardner and Spowart, 1990], 2) the droplet trajectories may be influenced by the laser beam itself when passing at a slower velocity [Nagel et al, 2007], and 3) the shape of the droplets may change when accelerated to a faster velocity [Wendisch et al, 1996], although Pruppacher and Beard [1970] found that droplets as large as 400 um experienced minimal physical deformation once the droplets have relaxed to a steady velocity. These effects could influence the measured pulse width and height in addition to the counting rate. The evaporation flow-tube and sheath flow rate used in these calibrations resulted in droplet velocities of 30-40 m $s^{-1}$ for droplets smaller than 25 um.

While these velocities are significantly lower than the aircraft velocity, they are high enough to prevent problem #2 above. Future work is planned using a flow-tube with a much longer flow-tube nozzle (~4 cm), to allow greater time for droplet acceleration prior to exit, so that we may more thoroughly explore the effect of droplet velocity on the CDP response.

The position of droplets within the sample area of single-particle forward scatter instruments can affect the measured size, as shown by previous researchers (e.g. [Wendisch et al., 1996; Schmidt et al, 2004]). By precisely controlling the horizontal positioning of the droplets in the sample area of the CDP during calibration (longitudinally along the axis of the laser beam and laterally across the laser beam), we evaluated the response of the instrument at different locations and experimentally determine the degree to which random distribution of droplets within the sample area will broaden droplet size distributions measured in flight.

## 3. Fundamental Laboratory Characterization of the CDP

### *3.1 Sizing*

The CDP was initially calibrated with both PSL spheres and glass beads. In addition to the standard CDP binned size distributions we also recorded the waveforms of electronic pulses corresponding to a sampling of individual particles as detected by the sizer and qualifier and measured with an oscilloscope. Figure 2a shows the calibrated sizer pulse amplitude, corresponding to the maximum amount of light collected for a droplet of a given size. Also plotted are the theoretically determined response functions of the CDP for different particle refractive indices, calculated from Mie theory. The range of collection angles for the theoretical curves illustrates the expected sensitivity of the CDP response to changes in the droplet position within the sample area. Glass beads were aspirated from a small vial and through a tube positioned over the sample area of the CDP using dry compressed gas. The PSL calibrations were performed using a nebulizer to generate droplets from PSL particles in water, followed by a diffusional dryer to evaporate the water from the PSL particles, and then transmitted across the sample area of the CDP using the evaporation flow-tube. For both the PSL and glass bead calibrations aggregation of generated particles is possible, which would result in a bias in the measured pulse amplitude. Coincidence is also possible, but is extremely unlikely for the PSL calibrations, since particle count rates were less than 0.1 Hz.

Calibrations of the CDP were also performed using monodisperse water droplets 8-35 um in diameter. Droplets were generated as detailed above, and injected through the CDP laser beam at the lateral and longitudinal position that produced the maximum sizing pulse amplitude. Once this position was located, calibration of various droplet sizes was performed. Figure 2a and 2b show the calibrated response of the CDP to water droplets; no averaging was performed and each data point represents a single droplet as measured by the metrology camera and by the oscilloscope. The response of the CDP to varying water droplet sizes is surprisingly monotonic, and unexpected from Mie theory, for reasons that are not known. From Figures 2a and 2b, it appears that the CDP has a general tendency to oversize droplets, especially for droplet sizes smaller than 20um, when using the glass bead and PSL particles for calibration. This may be because the calibration using water droplets is constrained to the center of the DoF where the scattered light signal is highest, whereas the glass beads and PSL particles are transmitted randomly across the CDP sample area giving a lower signal on average. By shifting the bin designations by 2 um, the CDP response is able to much better represent the true droplet diameter obtained from images of the droplet glares for droplets at the center of the DoF. Figure 2b shows the volume mean diameter ($D_V$, [Seinfeld and Pandis, 1998]) calculated from the droplet size distributions reported in the standard CDP measurement (with the threshold diameter in the CDP software representing the smallest diameter of each bin) as a function of the true droplet diameter obtained from images of the droplet glares. Droplets are oversized by up to 20% using the standard CDP diameter thresholds. As mentioned above, subtracting 2 um from each size bin produces much better agreement, with a slope of 0.977 ± 0.0013 (forced through the origin) and a linear correlation coefficient ($R^2$) of 0.994. Individual droplets 10-20 um in diameter may still be under or over sized by as much as 10% due to the coarse size resolution of the bins.

Figures 3a and 3b shows the CDP droplet sizing accuracy as a function of position within the qualified sample area, $SA_Q$, for two different droplet sizes (22 um and 12 um), after the 2um sizing offset has been applied. The measurements were obtained at regular intervals of 200 um along the axis of the laser beam and 20 um across the laser beam, with higher resolution at the edges of the qualified sample area (to within 50 um and 10 um, respectively) after the edge has been identified through the absence of counts on the CDP. The sizing variability within $SA_Q$ is large, with undersizing by as much as 74% possible as well as oversizing by as much as 12%, but only a small fraction of the area within $SA_Q$ results in undersizing by more than 25%. The most likely sizing bias within $SA_Q$ is -1.2% (-8.6% on average) for 12 um droplets and 0.6% (-2.4% on average) for 22 um droplets.

*3.2 Counting*

The standard CDP measurement provides a counting rate (droplets $s^{-1}$). For a given position within $SA_Q$, the measured counting rate is in close agreement with the rate at which droplets were generated with the piezo-electric actuator (250 Hz). At the edges of $SA_Q$, a higher or a lower counting rate is possible due to electronic noise, which becomes important when the qualifier and sizer signals have nearly the same amplitude (Figures 3b, 3d). The effect of electronic noise is also greater when the pulse amplitude is smaller, as when smaller droplets are used. $SA_Q$ integrated from the data shown in Figure 3 is $0.3 \pm 0.04$ $mm^2$ for both 12 and 22 um droplets, which is consistent with the manufacturer specifications. Although the counting rate varies significantly at the edges of $SA_Q$, the average counting rate within $SA_Q$ for both experiments is within 5% of the rate that droplets were generated.

## 4. In-Flight Performance of the CDP

*4.1 Comparison with in-situ LWC*

During a transit flight on March 29, 2008 from Tampa, FL to Denver, CO in preparation for the ARCPAC campaign, multiple warm (liquid), nonprecipitating clouds were intercepted at altitudes ranging from 900-1500 m over a period of about 1 hour. The observations made during this time period provide the basis for our LWC comparison. The measured droplet $D_V$ ranged from 4-17 um for these clouds with an average $D_V$ of 11.9 um (after shifting the size bins by 2 um, as described in Section 3.1), and droplet concentrations averaged 217 $cm^{-3}$ with a maximum of 436 $cm^{-3}$.

A bias was discovered in the CDP-LWC calculated from the measured droplet size distribution, as compared to the mass of liquid water measured by the hot-wire King probe (King-LWC). The CDP-LWC bias, defined as (CDP-LWC – King-LWC) / King-LWC, is strongly and linearly correlated with the measured droplet concentration (Figure 4). This bias is consistent throughout the transit flight, and is also shown to be consistent on other flights where liquid water is present. Because of the droplet concentration dependence, we hypothesize that coincidence errors are responsible for the observed discrepancy in LWC. To quantify the expected coincidence errors, we first determine $SA_E$ in the laboratory, and then perform Monte Carlo simulations to evaluate the effect of coincidence on measured droplet concentrations and droplet sizes. Section 5 gives an in-depth description of the method used for quantifying coincidence errors in the CDP.

*4.2 Ice- and Mixed-Phase- Clouds*

During an Arctic flight out of Fairbanks, AK on April 19th, 2008 we observed a much wider dynamic range in droplet concentrations than during the transit flight on March 29$^{th}$. However, many of the clouds sampled during this Arctic flight were mixed-phase clouds, with ice crystals as large as 1 mm and King-LWC as high as 0.3 g m$^{-3}$ simultaneously observed. Ice crystals can lead to measurement artifacts in at least two ways, 1) by biasing the hot-wire LWC measurements and 2) by shattering on the arms of the CDP and producing many small ice particles that are counted as liquid droplets. In spite of this, the CDP-LWC bias for this flight showed the same linear trend with droplet concentration as did the liquid-only clouds sampled on the transit flight. Both flights are shown in Figure 4. The robustness of this result over an even broader range of droplet concentrations gives us increased confidence that coincidence errors are driving the observed discrepancy between the CDP-LWC and the King-LWC. Furthermore, it suggests that ice crystal shattering did not significantly affect the CDP-LWC bias observed for these particular mixed-phase clouds.

Figure 5 shows the size distribution from the CDP (3-50um), the CIP (50-200um) and PIP (200-6000um) for a liquid-only cloud, two ice-only clouds, and two mixed-phase clouds on the April 19th, 2008 flight. The use of 1 Hz data in Figure 5 sets the minimum concentration observable by each instrument; the instrument counting limits are plotted in addition to the ambient size distributions. The liquid-only cloud shown has a skewed single-mode distribution with a peak in concentration at ~10 um droplet diameter. The two mixed-phase clouds have similar droplet distributions to the liquid-only cloud, with skewed Gaussian shapes that peak in concentrations between 10 and 30 um droplet diameters.

The absence of liquid droplets in ice-only clouds allows for a closer evaluation of ice crystal shattering on the CDP measurements. The ice-only condition is operationally defined when measured LWC is below the 0.1 g $m^{-3}$ detection limit of the King hot-wire probe. Ice-Only Cloud 1 in Figure 5 contained ice precipitation concentrations of ~2 $L^{-1}$, including many large (> 1 mm), lightly rimed, dendritic and aggregated ice crystals (as shown at the bottom of Fig. 5), which are expected to be the most fragile of any ice crystal habit [Pruppacher and Klett, 2000]. Yet these conditions result in very little effect on the CDP size distribution, with concentrations one to two orders of magnitude less than observed in liquid clouds at any given size between 8 and 50 um in diameter. The measured CDP concentration is less than 0.7 $cm^{-3}$ in this example, resulting in CDP-

LWC of only $2x10^{-5}$ g $m^{-3}$. In fact, it is not clear that the few particles observed by the CDP during this time period are fragments of shattered ice crystals, since liquid droplets this small and few in number would not be observable by the King-LWC probe. Despite this ambiguity, it is clear that the ice crystal shattering artifact in the CDP cannot be large for this example, even under the very poor conditions encountered. For Ice-Only Cloud 2 it is also unclear whether the much higher number concentration (~52 $L^{-1}$) of ice hydrometeors is affecting the CDP measurement, since the particles observed in the CDP are so small and few that their total volume cannot be verified by the King-LWC probe. The shape of the particle size distribution measured by the CDP, however, is similar to the distributions observed in liquid and mixed-phase clouds, suggesting that Ice-Only Cloud 2 may indeed be a mixed-phase cloud.

**5. Quantifying Coincidence Errors**

Both the qualified sample area, $SA_Q$, and the extended sample area, $SA_E$, must be known to quantify coincidence errors. We calibrate $SA_E$ in the same way that we calibrate $SA_Q$, by transmitting droplets at precise locations across the CDP laser beam and monitoring the instrument response. However, instead of monitoring the relative signals from the sizer and qualifier, only the sizer signal is recorded. At any position the sizer is able to detect droplets (even outside of $SA_Q$), the potential exists for coincident droplets to affect the sizing and counting of qualified droplets. $SA_E$ is much larger than $SA_Q$, spanning more than 2 cm, or roughly half the distance between the arms of the CDP (Figure 6).

To simulate the effect of coincidence errors on the CDP performance, we developed a Monte Carlo program with two distinct time scales, one for qualified droplets transiting through $SA_Q$ and one for coincident droplets transiting through $SA_E$. In the simulations, first an input droplet size distribution is prescribed, and individual droplets within this distribution transit the CDP laser at random time intervals and positions. The time interval between droplets is constrained by the ranges $0 < \delta t < 2\tau_Q$ and $0 < \delta t < 2\tau_C$ for qualified and coincident droplets, respectively, as

$$\tau_Q = 1 / n_D$$

$$\tau_C = (1 / n_D)\ (SA_Q / SA_E)$$

where $\delta t$ is the time between individual droplets, $\tau_C$ is the average time between coincident droplets (s), $\tau_Q$ is the average time between qualified droplets (s), and $n_D$ is the prescribed qualified droplet counting rate (drops/s). All time intervals between 0 and $2\tau$ are considered equally likely, yet the average time interval between droplets remains $\tau$. Likewise, transit of droplets across any position within $SA_Q$ and $SA_E$ is considered equally likely.

At 100 m $s^{-1}$ flight speed, droplets pass through the ~0.2 mm diameter laser beam in ~2 us. The average transit time of qualified droplets is determined by the duration for which the simulated sizer signal exceeds a threshold of 20 digital counts until the sizer signal drops below 10 digital counts (as long as the qualifier signal exceeds the sizer signal at some point during this time period). For a series of coincident droplets, the transit time configured in this way can be very long, and can therefore be used as a diagnostic for in-flight coincidence errors. We use a time window of 100 us in the simulations to allow for long transit times, so that we can evaluate this diagnostic parameter. The average transit time is linked to the pulse widths of individual droplets (defined as twice the Gaussian standard deviation of the pulse), which is not known precisely since it depends on multiple factors including the width of the laser beam at a given location, the droplet size, and the aircraft velocity. Wider pulses result in greater overlap between pulses, which means that there is less time for the sizer signal to relax back to its baseline thereby terminating the transit time. Thus, the average transit time constrains the pulse widths that can be used in the simulations. This constraint is also important because the simulations also show that the pulse width of individual droplets can strongly affect the coincidence error. Measured pulse widths during the water droplet calibrations ranged from 2-5 us, for droplets 8-35 um in diameter traveling at roughly 30% of the NOAA WP-3D velocity. Therefore, we expect a range of pulse widths roughly 0.5-1.5 us during the ARCPAC campaign.

The measured response of the sizer and qualifier to individual droplets within $SA_Q$ and $SA_E$ during the laboratory calibrations constrains the simulated sizing and counting errors of the CDP. In the simulations, droplets are individually allowed to transit randomly across $SA_Q$, and the pulse amplitude is then modified depending on the position of the droplet within $SA_Q$. Simultaneously, other droplets may randomly transit across $SA_E$, whereby simulated pulses are generated with amplitudes that depend on their position within $SA_E$. The qualifier and sizer signals for all droplets transiting across $SA_E$ and $SA_Q$ are then summed. We assume in the simulations that the scattered light from one droplet does not affect the scattering response of any other droplet.

Figure 7 shows examples of simulated sizer and qualifier signals, with the prescribed qualified droplet positioned at the center of the 100 us time window. A "perfect" instrument is one in which the pulse amplitude is unaffected by coincidence or inhomogeneous instrument response, and is instead directly and unambiguously related to droplet size according to the power law relationship shown in Figure 2a. In actuality, for an imperfect instrument, several different results are possible:

7a) The qualified droplet is undersized after transiting through a position within $SA_Q$ with a lower response. The droplet size is unaffected by coincidence for this particular case because no coincident droplets happened to arrive at exactly the same time as the qualified droplet. However, the transit time for this case is slightly longer than it would have been, because coincidence extends the amount of time that the sizer signal remains above an electronic threshold.

7b) The droplet is oversized due to a coincident droplet that scatters additional light into the sizer. In this case, the transit time is also much longer due to several other coincident droplets.

7c) The sizer signal exceeds the qualifier signal due to a coincident droplet, resulting in erroneous rejection of the qualified droplet. The maximum oversizing error due to coincidence is constrained by the qualifier signal; when this constraint is exceeded, droplets are undercounted.

The droplet size can also be important in simulating the effect of coincidence. Doubling the pulse signal voltage (the maximum effect possible due to extended coincidence, since the maximum qualifier/sizer signal ratio is ~2) has a greater effect on the measured droplet size when the droplets are small. As an example, doubling the voltage from 195 to 390 mV represents an increase in droplet diameter from 6.4 to 13.2 um (a 106% increase), whereas doubling the voltage from 372 to 744 mV represents an increase in droplet diameter from 12.6 to 21.2 um (a 68% increase). This means that 6.4 um droplets can have up to 38% greater oversizing error due to coincidence than 12.6 um droplets. In terms of the relative increase in LWC, the effect can be much larger. This does not account for the effect of pulse width, which is expected to be droplet size dependent.

We ran the simulations with 500 qualified droplets for prescribed droplet concentrations ranging from 50 to 550 $cm^{-3}$. Figure 8a shows the simulated bias in $D_V$ for a range of droplet sizes, pulse widths and droplet concentrations. The linear fits of the simulated $D_V$ error as a function of the prescribed droplet concentration are shown for two sets of simulation; the slope of these lines decreases with increasing droplet size, as expected due to the nonlinear relationship between forward scatter intensity and droplet size. The oversizing bias due to coincidence is simulated to range from 5% per 100 $cm^{-3}$ droplet concentrations to as high as 13% per 100 $cm^{-3}$, for droplet sizes from ~5 um to ~12 um, resulting in as much as 60% oversizing bias at droplet concentrations of 500 $cm^{-3}$. Undercounting resulting from coincidence is similarly dramatic, as shown in Figure 8b, with undercounting as high as 50% in the simulations for prescribed droplet concentrations of 500 $cm^{-3}$. The undercounting error due to coincidence is not strongly dependent on droplet size, but is affected by the pulse widths used in the simulations. As mentioned, the pulse widths and droplet sizes are independently varied in the simulations, although in reality they are not entirely independent from one another.

The instrument response is simulated by binning the pulse amplitudes according to the standard CDP size bins (shifted by 2um, as done with the ambient measurements). Figure 9 shows simulated droplet size distributions at different prescribed droplet concentrations. At low droplet concentrations (Figure 9a) the simulated droplet size distribution is not significantly affected by coincidence, and the breadth of the simulated distribution is instead controlled by the variable response of the CDP to droplets within $SA_Q$. At higher droplet concentrations, the effect of coincidence broadens and shifts the droplet size distribution to larger sizes (Figure 9b). Ambient droplet size distributions observed during a flight during ARCPAC are shown for comparison to the simulated size distributions, in Figures 9a and 9b. The simulated and measured size distributions and CDP-LWC biases are comparable for these examples, illustrating the plausibility of the prescribed droplet distributions used in both simulations.

For direct comparison to the ambient observations (Figure 4), the simulated CDP-LWC bias is calculated and plotted as a function of the simulated droplet concentration (Figure 10). At low droplet concentrations the simulations reproduce the in-flight negative CDP-LWC bias that results from the inhomogeneous response of the CDP to droplets within $SA_Q$. This is the expected result of using the water droplet calibrations at the center of the DoF to determine the size of droplets that are distributed throughout the qualified sample area.

Extended coincidence causes the simulated CDP-LWC bias to increase with droplet concentration in Figure 10. The slope of this relationship is strongly dependent on the droplet size and pulse widths prescribed in the simulations. Simulations with droplets diameters of 5-9 um appear to explain the observed slope, given prescribed pulse widths of 1.5-2.0 us constrained by average transit time observations. Simulations with prescribed droplet sizes larger than 9 um result in lower CDP-LWC bias than observed for droplet concentrations as low as 150 $cm^{-3}$. This result is consistent with the fact that high droplet concentrations are typically correlated with smaller droplet sizes in ambient clouds due to the limited amount of liquid water distributed among the droplets. During ARCPAC, observed $D_V$ ranged from 11 um on average for measured droplet concentrations greater than 300 $cm^{-3}$ to 15 um on average for droplet concentrations less than 100 $cm^{-3}$. The simulations show that during events of high droplet concentrations, the droplet size is actually much smaller and the distribution is narrower than the measurements indicate, as illustrated in Figure 9b.

Figure 11 shows the average transit times derived from the simulations compared to the observations. The simulations reproduce the general trend of increasing transit time at higher droplet concentrations. At the low droplet concentrations the simulated transit time is slightly longer than the observations, suggesting that shorter pulse widths should be used in the simulations. However, at high droplet concentrations, the simulated transit times are lower than many of the observations, suggesting that the effect of coincidence can be much more pronounced than we have simulated.

It is important to note that heterogeneity in droplet concentrations over time intervals smaller than the 1 second sampling period will always increase the coincidence errors for a given measured droplet concentration. We ran additional simulations with a droplet counting rate that varied within the 1 second sampling period: 1) assuming that all droplets arrived, randomly, in the qualified sample area during the first half of the sampling period (L = 50m, where L is the length scale of the cloud filament) and 2) assuming that the droplets all arrived during the first third of the sampling period (L= 33m). The result of these simulations is greater oversizing and greater undercounting errors due to coincidence for a given droplet size, even with smaller prescribed pulse widths (as shown in Figures 8a and 8b). It is impossible to resolve or correct for variability in droplet concentrations at horizontal scales smaller than 100 m for the ARCPAC dataset (assuming an aircraft velocity of 100 m $s^{-1}$), since sampling rates higher than 1Hz were not obtained. However, by incorporating sub-sample variability in droplet concentrations into the simulations, we are able to simultaneously account for the range of CDP-LWC biases, droplet sizes and the large average transit times observed at measured droplet concentrations less than 400 $cm^{-3}$.

## 6. Summary and Conclusions

Laboratory calibrations of the CDP sample area and droplet sizing were performed using water droplets of known size and concentration. However, comparison with an independent measure of liquid water content (LWC) in-flight suggests a bias in the droplet size and/or droplet concentration measured by the CDP that are beyond the uncertainties determined from the laboratory calibrations. Since the bias in CDP-LWC is strongly concentration dependent, we hypothesize that the discrepancy is a result of coincidence, when two or more droplets pass through the CDP laser beam within a very short time of each other. The coincidence error is evaluated in terms of an extended sample area, the area in which individual droplets can affect the sizing detector without necessarily registering as a valid droplet.

A Monte-Carlo simulation was developed to estimate the effect of coincidence on the measured droplet size distributions based on laboratory calibrations of the extended sample area using water droplets. The simulations show that coincidence errors can explain two distinct trends in the ambient observations: 1) the observed increase in CDP-LWC bias as a function of droplet concentrations, and 2) the increase in average transit time as a function of droplet concentrations. Coincidence was found to be significant for the CDP at droplet concentrations even as low as 200 $cm^{-3}$. We estimate that 60% oversizing and 50% undercounting due to coincidence can occur in the CDP at droplet concentrations of 500 $cm^{-3}$, and expect that these biases are dependent on the droplet size. We show that the simulations can replicate specific observed droplet size distributions and concentrations while also producing CDP-LWC biases consistent with the observations. However, many of the observed droplet sizes are too large to be explained in the simulations, and the initial simulations are also unable to reproduce many of the very high average transit times observed. This suggests that, at times, there is an even greater effect of coincidence than expected. We show that one possible reason for greater coincidence errors is spatial variability in ambient droplet concentrations at horizontal scales smaller than can be resolved for the 1Hz measurements obtained. It should be emphasized that, ultimately, the simulations provide only plausible scenarios and general tendencies, rather than absolute correction factors for specific size distribution measurements, due to insufficient constraints on the actual size and pulse widths of individual droplets as well as unresolved spatial heterogeneity in droplet concentrations.

Having identified a weakness in the CDP optical design, the primary goal at this stage is to minimize coincidence errors as much as possible by physically modifying the CDP optics to limit the area viewable by the sizing detector. Such a modest change is expected to greatly reduce measurement biases in droplet concentration and size. These changes are being pursued prior to further field use of the instrument and will be the subject of future laboratory and field evaluations.

**Acknowledgements**

This work was supported by the National Oceanic and Atmospheric Administration (NOAA) climate and air quality programs. We thank Jorge Delgado and the NOAA Aircraft Operations Center for allowing use of their equipment and for technical support in the field. We thank Bill Dubé and Matt Richardson for practical laboratory support. We give special thanks to Alexei Korolev, Dan Murphy, and Al Cooper for critical comments and advice. S. Lance thanks the National Research Council for a Research Associateships Program fellowship awarded in January 2008, and further thanks the Cooperative Institute for Research in Environmental Sciences, University of Colorado, Boulder.

**References**

Alekseev, G.V., A. I. Danilov, V. M. Kattsov, S. I. Kuz'mina and N. E. Ivanov, Changes in the Climate and Sea Ice of the Northern Hemisphere in the 20th and 21st Centuries from Data of Observations and Modeling, *Atmos. Oceanic Phys*., 45 (6), 723–735, 2009.

Baumgardner, D., and M. Spowart, Evaluation of the Forward Scattering Spectrometer Probe. Part III: Time Response and Laser Imhomogeneity Limitations, *J. Atmos. Oceanic Technol*., 7, 666-672, 1990.

Baumgardner, D., W. Strapp, and J.E. Dye, Evaluation of the Forward Scattering Spectrometer Probe. Part II: Corrections for coincidence and dead-time losses. *J. Atmos. Oceanic Technol*., 2, 626-632, 1985.

Baumgardner, D., An Analysis and Comparison of Five Water Droplet Measuring Instruments, *J. Climate Appl. Met*., 22, 891-910, 1983.

Biter, C.J., J.E. Dye, D. Huffman and W.D. King, The Drop-Size Response of the CSIRO Liquid Water Probe, *J. Atmos. Oceanic Technol*., 4, 359-367, 1987.

Bohren, C.F. and D.R. Huffman, Absorption and Scattering of Light by Small Particles, John Wiley and Sons, 1983.

Brenguier, J.L., D. Baumgardner and B. Baker, A Review and Discussion of Processing Algorithms for FSSP Concentration Measurements, *J. Atmos. Oceanic Technol*., Notes and Correspondence, 11, 1409-1414, 1994.

Brenguier, J.L., T. Bourrianne, A. de A. Coelho, J. Isbert, R. Peytavi, D. Trevarin, P. Weschler, Improvements of Droplet Size Distribution Measurements with the Fast-FSSP (Forward Scattering Spectrometer Probe), *J. Atmos. Oceanic Technol*., 15, 1077-1090, 1998.

Brock, C.A., J. Cozic, R. Bahreini, J. Brioude, J.A. de Gouw, D.W. Fahey, R. Ferrare, K.D. Froyd, J.S. Holloway, G. Hübler, D. Lack, S. Lance, A.M. Middlebrook, S.A. Montzka, D.M. Murphy, J.A. Neuman, J. Nowak, J. Peischl, B. Pierce, T.B. Ryerson, J.P.

Schwarz, H. Sodemann, R. Spackman, B. Stocks, A. Stohl, P. Veres and C. Warneke, Characteristics, Sources, and Transport of Aerosols Measured in Spring 2008 During the Aerosol, Radiation, and Cloud Processes Affecting Arctic Climate (ARCPAC) Project, *in preparation*.

Burnet, F. and J.-L. Brenguier, Comparison between Standard and Modified Forward Scattering Spectrometer Probes during the Small Cumulus Microphysics Study, *J. Atmos. Oceanic Technol*., 19, 1516-1531, 2002.

Conant W.C., T.M. VanReken, T.A. Rissman, V. Varutbangkul, H.H. Jonsson, A. Nenes, J.L. Jimenez, A.E. Delia, R. Bahreini, G.C. Roberts, R.C. Flagan, and J. H. Seinfeld, Aerosol-- cloud drop concentration closure in warm cumulus, *J. Geophys. Res*., 109, D13204, doi:10.1029/2003JD004324, 2004.

Cooper, W.A., Effects of Coincidence on Measurements with a Forward Scattering Spectrometer Probe, *J. Atmos. Ocean. Technol*., 5, 823-832, 1988.

Curry, J.A., J.L.Schramm and E.E. Ebert, Impact of Clouds on the Surface Radiation Balance of the Arctic Ocean, *Meteorology and Atmospheric Physics*, 51, 197-217, 1993.

Curry, J.A., and E.E. Ebert, Annual Cycle of Radiation Fluxes over the Arctic Ocean: Sensitivity to Cloud Optical Properties, *J. Climate*, 5, 1267-1280, 1992.

Diehl, K., G. Huber, S.K. Mitra and M. Wendisch, Laboratory Studies of Scattering Properties of Polluted Cloud Droplets: Implications for FSSP Measurements, *J. Atmos. Oceanic Technol*., 25, 1894-1898, 2008.

Feind, R.E., A.G. Detwiler, and P.L. Smith, Cloud Liquid Water Measurements on the Armored T-28: Intercomparison between Johnson–Williams Cloud Water Meter and CSIRO (King) Liquid Water Probe, J. Atmos. Oceanic Technol., 17, 1630-1638, 2000.

Feingold, G., R. Furrer, P. Pilewskie, L.A. Remer, Q. Min and H. Jonsson, Aerosol Indirect Effect Studies at Southern Great Plains during the May 2003 Intensive Operations Period, *J. Geophys. Res.*, 111, D05S14, doi:10.1029/2004JD005648, 2006.

Field, P.R., A.J. Heymsfield, and A. Bansemer, Shattering and Particle Interarrival Times Measured by Optical Array Probes in Ice Clouds, *J. Atmos. Oceanic Technol*., 23, 1357-1371, 2006.

Fountoukis, C., A. Nenes, N. Meskhidze, R. Bahreini,W.C. Conant, H. Jonsson, S. Murphy, A. Sorooshian, V. Varutbangkul, F. Brechtel, R.C. Flagan, and J.H. Seinfeld, Aerosol–cloud drop concentration closure for clouds sampled during the International Consortium for Atmospheric Research on Transport and Transformation 2004 campaign, *J. Geophys. Res.*, 112, D10S30, doi:10.1029/2006JD007272, 2007.

Garrett, T.J. and C. Zhao, Increased Arctic Cloud Longwave Emissivity Associated with Pollution from Mid-Latitudes, *Nature Letters*, 440, 787-789, 2006.

Heymsfield, A.J., On Measurements of Small Ice Particles in Clouds, *Geophys. Res. Lett*., 34, L23812, doi:10.1029/2007GL030951, 2007.

Hovenac, E.A. and J.A. Lock, Calibration of the Forward-Scattering Spectrometer Probe: Modeling Scattering from a Multimode Laser Beam, *J. Atmos. Oceanic Technol*., 10, 518-525, 1993.

Jensen, E.J., P. Lawson, B. Baker, B. Pilson, Q. Mo, A.J. Heymsfield, A. Bansemer, T.P. Bui, M. McGill, D. Hlavka, G. Heymsfield, S. Platnick, G. T. Arnold, and S. Tanelli, On the importance of small ice crystals in tropical anvil cirrus, *Atmos. Chem. Phys*., 9, 5519–5537, 2009.

Jonnson, H. and B. Vonnegut, Technique for Producing Uniform Small Droplets by Capillary Waves Excited in a Meniscus, *Rev. Sci. Instrum*., 53, 1915-1919, 1982.

King, W.D., J.E. Dye, J.W. Strapp, D. Baumgardner and D. Huffman, Icing Wind Tunnel Tests on the CSIRO Liquid Water Probe, *J. Oceanic Atmos. Technol*, 2, 340-352, 1985.

King , W.D., C.T. Maher and G.A. Hepburn, Further Performance Tests on the CSIRO Liquid Water Probe, *J. Appl. Meteor*., 20, 195-202, 1981.

King , W.D., D.A. Parkin and R.J. Handsworth, A Hot-Wire Liquid Water Device having Fully Calculable Response Characteristics, *J. Appl. Meteor.*, 1809-1813, 1978

Knollenberg, R.G., Practical Applications of Low Power Lasers , *SPIE*, 92, 137-152, 1976.

Korolev, A. V., Yu. E. Makarov, and V. S. Novikov, 1985: On the accuracy of photoelectric cloud droplet spectrometer FSSP-100 (in Russian). *Tr. Tsentr. Aerol. Obs.*, 158, 32–49. [English translation available online at http://www.skytechresearch.com/news.htm.]

Korolev, A.V., S.V. Kuznetsov, Y.E. Makarov and V.S. Novikov, Evaluation of Measurements of Particle Size and Sample Area from Optical Array Probes, *J. Atmos. Oceanic Technol.*, 8, 514-522, 1991.

Korolev, A. and G.A. Isaac, Shattering During Sampling by OAPs and HVPS. Part I: Snow Particles, *J. Atmos. Oceanic Technol.*, 22, 528-542, 2005.

Korolev, A.V., E.F. Emery, J.W. Strapp, S.G. Cober, G.A. Isaac, M. Wasey, B. Baker, R.P. Lawson, Small ice particle observations in tropospheric clouds: fact or artifact? Airborne Icing Instrumentation Evaluation Experiment, *in preparation*.

Lee, E.R., Microdrop Generation, CRC Press LLC, Boca Raton, FL, 2003.

Lubin, D., and A.M. Vogelmann, A Climatologically Significant Aerosol Longwave Indirect Effect in the Arctic, *Nature*, 439, 453-456, doi:10.1038, 2006.

McConnell, J.R., R. Edwards, G. L. Kok, M.G. Flanner, C.S. Zender, E.S. Saltzman, J.R. Banta, D.R. Pasteris, M.M. Carter, J.D.W. Kahl, 20th-Century Industrial Black Carbon Emissions Altered Arctic Climate Forcing, *Science*, 317, 1381-1384, 2007.

McFarquahar, G.M., J. Um, M. Freer, D. Baumgardner, G.L. Kok, and G. Mace, Importance of Small Ice Crystals to Cirrus Properties: Observations from the Tropical Warm Pool International Cloud Experiment, *Geophys. Res. Lett.*, 34, L13803, doi: 10.1029/2007GL029865, 2007.

Meskhidze, N., A. Nenes, W.C. Conant, and J.H. Seinfeld, Evaluation of a new cloud droplet activation parameterization with in situ data from CRYSTAL-FACE and CSTRIPE, *J. Geophys. Res*., 110, D16202, doi:10.1029/2004JD005703, 2005.

Nagel, D., U. Maixner, W. Strapp and M. Wasey, Advancements in Techniques for Calibration and Characterization of In Situ Optical Particle Measuring Probes, and Applications to the FSSP-100 Probe, *J. Atmos. Oceanic Technol.*, 24, 745-760, DOI: 10.1175/JTECH2006.1, 2007.

Pruppacher, H.R. and K.V Beard, A Wind Tunnel Investigation of the Internal Circulation and Shape of Water Drops Falling at Terminal Velocity in Air, *Quart. J. R. Met. Soc., 96*, 247-256, 1970.

Pruppacher, H.R. and J.D. Klett, Microphysics of Clouds and Precipitation, 2$^{nd}$ Ed., Kluwer Academic Publishers, the Netherlands, 2000.

Schafer, J., J.P. Mondia, R. Sharma, Z.H. Lu, and L.J. Wang, Modular Microdrop Generator, Rev. Sci. Instrum., 78, DOI: 10.1063/1.2742809, 2007.

Schmidt, S., K. Lehmann, and M. Wendisch, Minimizing Instrumental Broadening of the Drop Size Distribution with the M-Fast-FSSP, *J. Oceanic Atmos. Technol*, 21, 1855-1867, 2004.

Schneider, J. M., and C. D. Hendricks, Source of Uniform Sized Liquid Droplets. *Rev. Sci. Instrum*., 35, 1349–1350, 1964.

Seinfeld, J.H. and S.N. Pandis, Atmospheric Chemistry and Physics, from Air Pollution to Climate Change, John Wiley and Sons, Inc., New York, 1998.

Serreze, M.C. and J.A. Francis, The Arctic Amplification Debate, *Climate Change*, 76 (3-4), 241-264, 2006.

Wendisch, M., A. Keil and A.V. Korolev, FSSP Characterization with Monodisperse Water Droplets, *J. Atmos. Oceanic Technol*., 13, 1152-1165, 1996.

**Figures**

**Figure 1.** a) Photograph of a single droplet in the sample area of the CDP, seen at an angle of 130 degrees from incident, using a shutter speed of 1/300,000 $s^{-1}$ (top). Photograph of the evaporation flow-tube positioned above the sample area of the CDP during calibration with water droplets (bottom), b) diagram of the glass evaporation flow-tube used in water droplet calibrations of the CDP, c) Top down view of the calibration setup, with the arms of the CDP (in yellow) pointing upwards.

**Figure 2.** a) CDP pulse height voltage (in milliVolts, on the right axis) versus the "true" droplet diameter (obtained from images of the droplet glares) within the sample area of the CDP for calibrations using glass beads, polystyrene latex spheres and water droplets. Also plotted are the theoretical response functions of the CDP (in Watts, on the left axis) as a function of droplet diameter, calculated using a given range of collection angles and refractive indices. The scales on each of the axes are adjusted to obtain alignment between the calibrations and the theoretical curves. b) volume mean diameter ($D_V$) from the standard CDP measurement versus $D_{true}$ determined from images of the droplet glares. Uncertainties in the glass bead and PSL particle sizes in Figure 2a represent one standard deviation as provided by Fischer Scientific, Inc. Uncertainties in the pulse amplitude are one standard deviation of the observed pulse amplitudes.

**Figure 3.** Calibrated CDP sizing and counting response as a function of lateral and longitudinal position using 22 um (a and c) and 12 um (b and d) water drops, at 35-40 m $s^{-1}$ velocity.

**Figure 4.** CDP-LWC bias, defined as (CDP-LWC – King-LWC) / King-LWC, for 1Hz measurements in liquid-only clouds on transit flight from Tampa to Denver on 3/29/2008 and in mixed-phase clouds on 4/19/2008 ARCPAC flight. Grey shaded region shows one standard deviation of the observations.

**Figure 5.** Example cloud particle size distributions (derived from CDP, CIP and PIP measurements) for liquid-only, ice-only and mixed-phase clouds on the 4/19/2008 ARCPAC flight. Also shown are images from the PIP for Ice-Only Cloud 1.

**Figure 6.** Calibration of the Qualified Sample Area ($SA_Q$) and Extended Sample Area ($SA_E$) for 22 um water droplets. Longitudinal direction is along the laser beam. Lateral direction is across the laser beam. The color scale shows the sizer amplitude for droplets transiting through that location, normalized to the maximum sizer amplitude at the center of the DoF.

**Figure 7.** Simulated electronic pulses at various droplet concentrations, constrained by water droplet calibrations of the CDP, for three different scenarios: a) qualified droplet is undersized due to transit through a location of less sensitive instrument response within $SA_Q$, b) qualified droplet is oversized due to coincident droplets, c) qualified droplet is not counted due to coincident droplets.

**Figure 8.** Simulated error in volume mean diameter ($D_V$) and droplet concentration as a function of prescribed droplet concentrations.

**Figure 9.** Prescribed and simulated droplet size distributions at droplet concentrations of a) 55 $cm^{-3}$ and b) 550 $cm^{-3}$. The simulations use prescribed droplet volume mean diameters and constant pulse widths of a) 12.6 um and 1.5 us, and b) 6.4 um and 1.8 us, respectively. The simulated CDP-LWC bias for each of these two cases is consistent with the range of CDP-LWC biases observed at a given droplet concentration during the 4/19/2008 ARCPAC flight. Also shown, for comparison, are 1 Hz droplet size distributions at comparable droplet concentrations, as measured during the 4/19/2008 flight.

**Figure 10**. Simulated bias in CDP-LWC as a result of laser intensity inhomogeneity within $SA_Q$ and as a result of coincidence errors, plotted as a function of droplet concentration. Plotted for comparison is the observed range (one standard deviation) in CDP-LWC bias (as compared to King-LWC) versus droplet concentration for the 4/19/2008 ARCPAC flight. Compare to actual data in Figure 4.

**Figure 11.** Simulated and observed average transit time as a function of the simulated and observed droplet concentrations.

**Figure 1.**

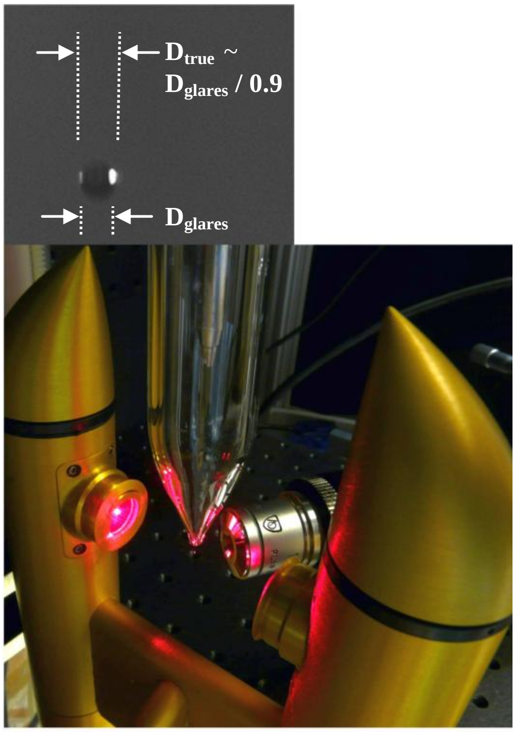

D_true ~
D_glares / 0.9
D_glares


**(a)**

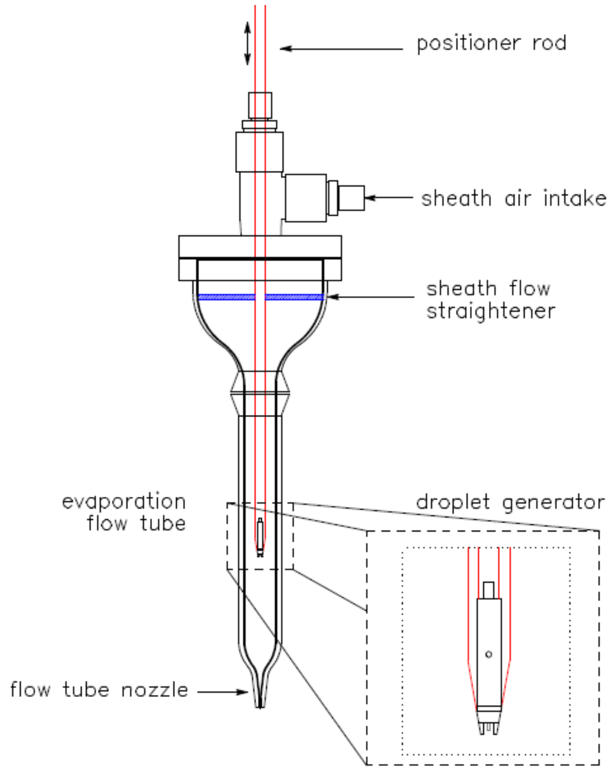

positioner rod
sheath air intake
sheath flow
straightener
evaporation
flow tube
droplet generator
flow tube nozzle


**(b)**

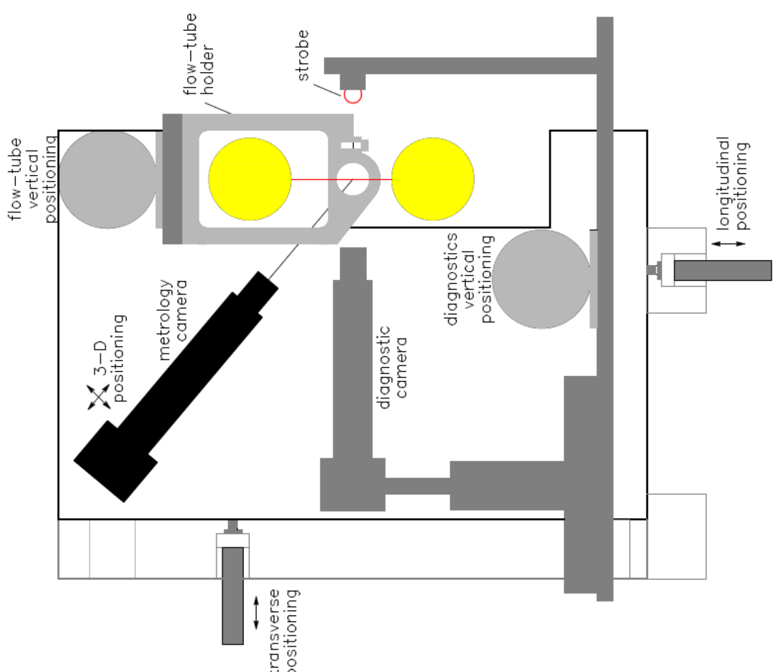

flow–tube
holder
strobe
flow–tube
vertical
positioning
longitudinal
positioning
diagnostics
vertical
positioning
metrology
camera
3–D
positioning
diagnostic
camera
transverse
positioning


**(c)**

**Figure 2.**

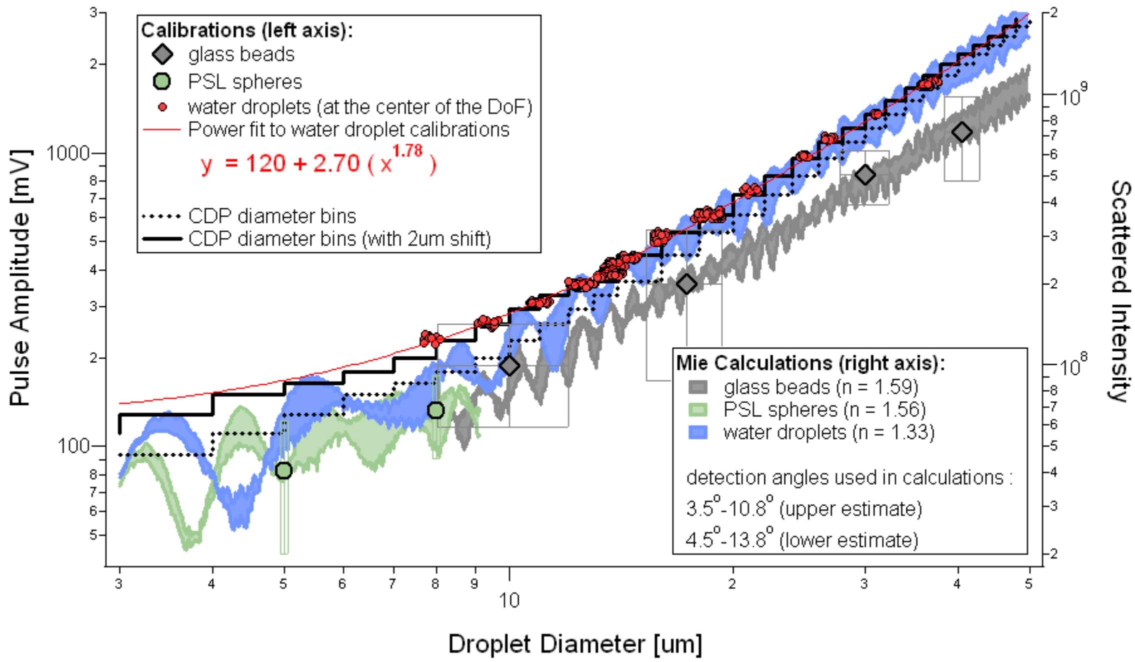
Calibrations (left axis):
glass beads
PSL spheres
water droplets (at the center of the DoF)
Power fit to water droplet calibrations
y = 120 + 2.70 ( x^1.78 )
CDP diameter bins
CDP diameter bins (with 2um shift)
Mie Calculations (right axis):
glass beads (n = 1.59)
PSL spheres (n = 1.56)
water droplets (n = 1.33)
detection angles used in calculations :
3.5°-10.8° (upper estimate)
4.5°-13.8° (lower estimate)
Pulse Amplitude [mV]
Scattered Intensity
Droplet Diameter [um]

**(a)**

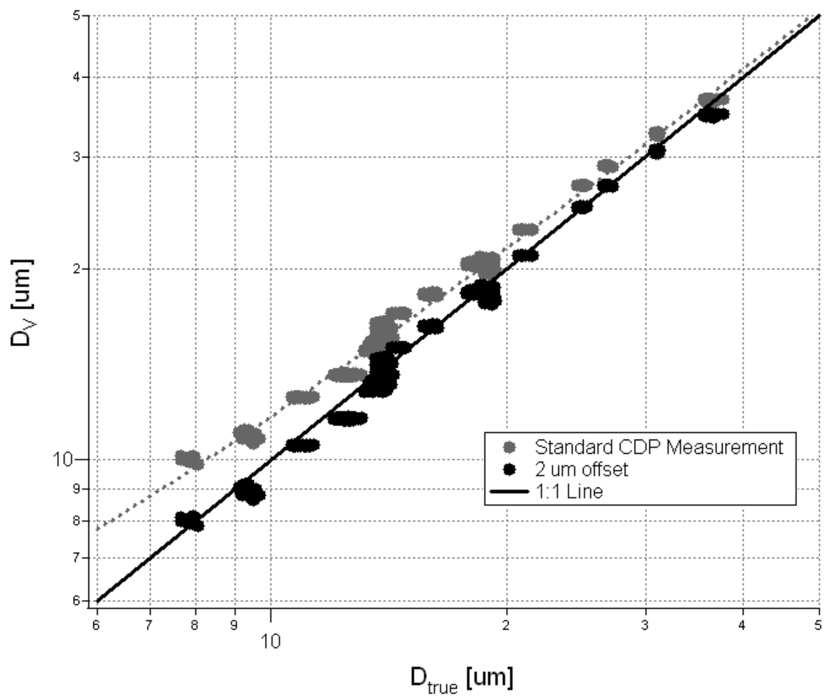
Standard CDP Measurement
2 um offset
1:1 Line
D_V [um]
D_true [um]

**(b)**

**Figure 3.**

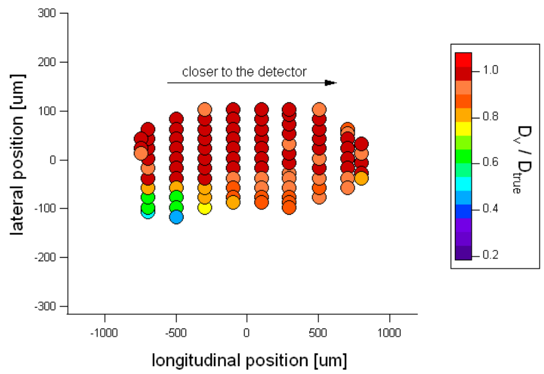


**(a)**

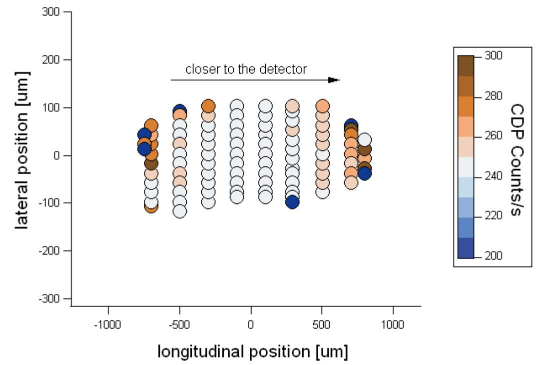


**(b)**

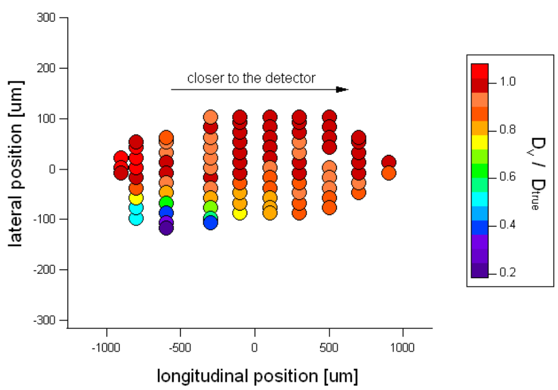


**(c)**

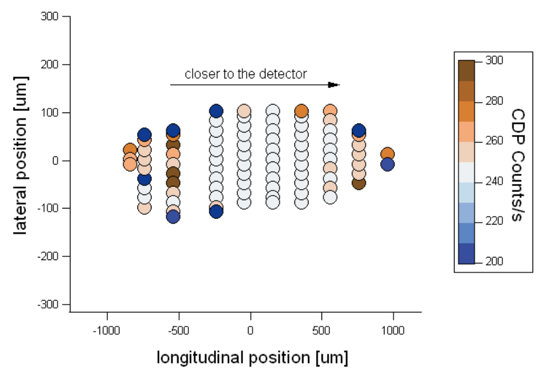


**(d)**

**Figure 4.**

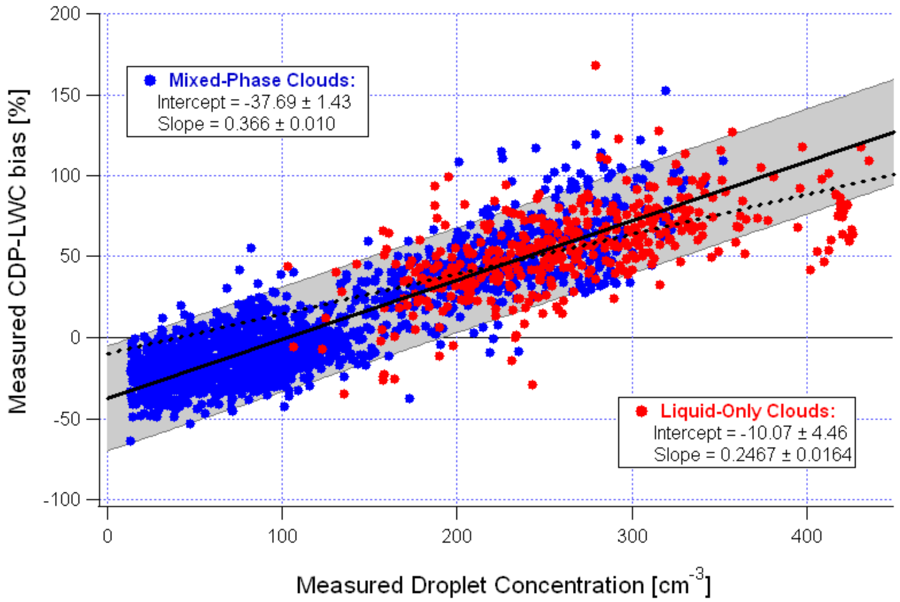
Mixed-Phase Clouds:
Intercept = -37.69 ± 1.43
Slope = 0.366 ± 0.010
Liquid-Only Clouds:
Intercept = -10.07 ± 4.46
Slope = 0.2467 ± 0.0164
Measured CDP-LWC bias [%]
Measured Droplet Concentration [cm-3]
200
150
100
50
0
-50
-100
0
100
200
300
400

**Figure 5.**

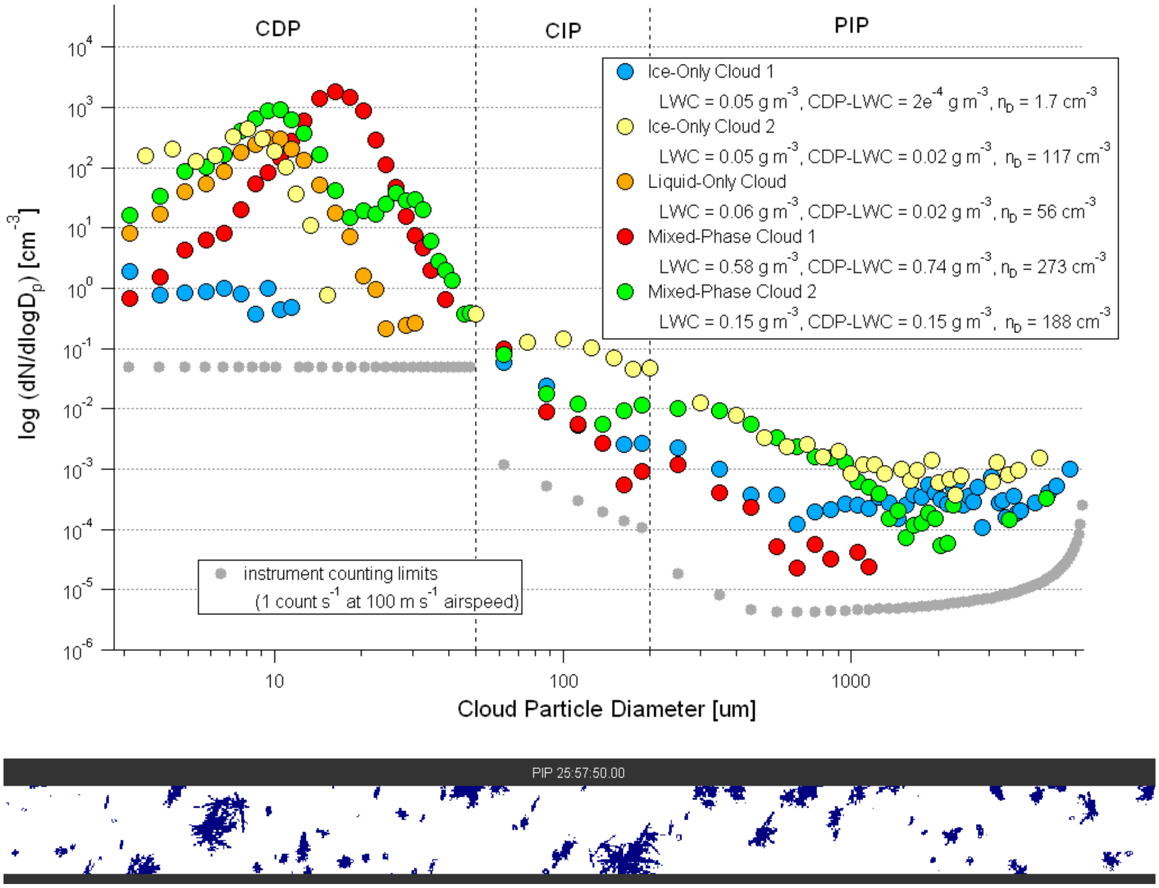
CDP
CIP
PIP
Ice-Only Cloud 1
LWC = 0.05 g m-3, CDP-LWC = 2e-4 g m-3, nD = 1.7 cm-3
Ice-Only Cloud 2
LWC = 0.05 g m-3, CDP-LWC = 0.02 g m-3, nD = 117 cm-3
Liquid-Only Cloud
LWC = 0.06 g m-3, CDP-LWC = 0.02 g m-3, nD = 56 cm-3
Mixed-Phase Cloud 1
LWC = 0.58 g m-3, CDP-LWC = 0.74 g m-3, nD = 273 cm-3
Mixed-Phase Cloud 2
LWC = 0.15 g m-3, CDP-LWC = 0.15 g m-3, nD = 188 cm-3
instrument counting limits
(1 count s-1 at 100 m s-1 airspeed)
log (dN/dlogDp) [cm-3]
Cloud Particle Diameter [um]
10
100
1000
PIP 25:57:50.00

**Figure 6.**

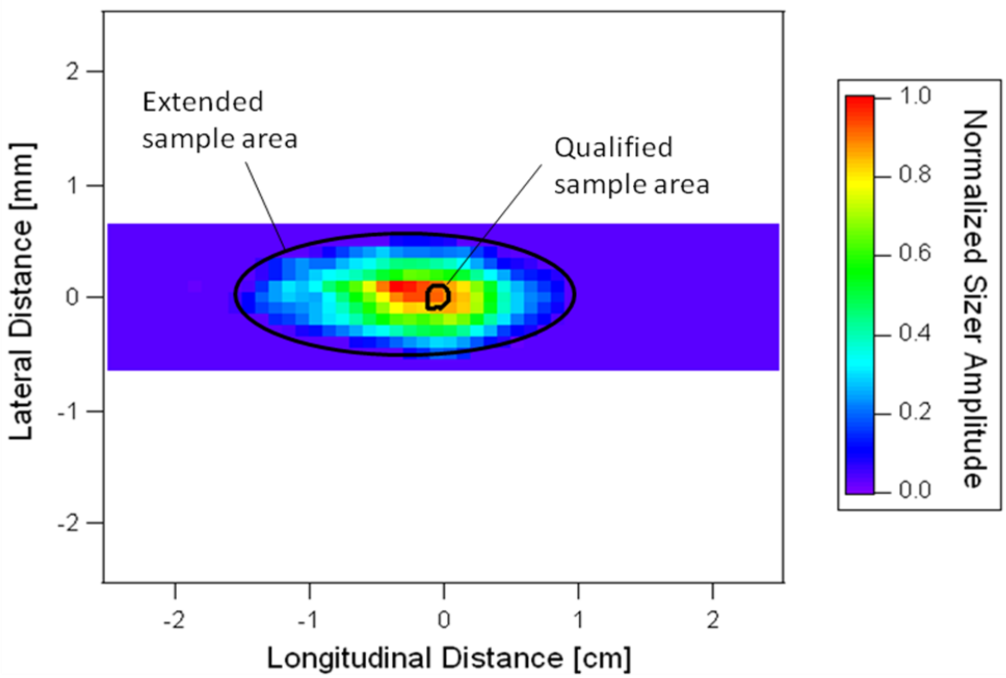

Extended sample area
Qualified sample area
Normalized Sizer Amplitude
1.0
0.8
0.6
0.4
0.2
0.0
Lateral Distance [mm]
2
1
0
-1
-2
Longitudinal Distance [cm]
-2
-1
0
1
2

Figure 7.

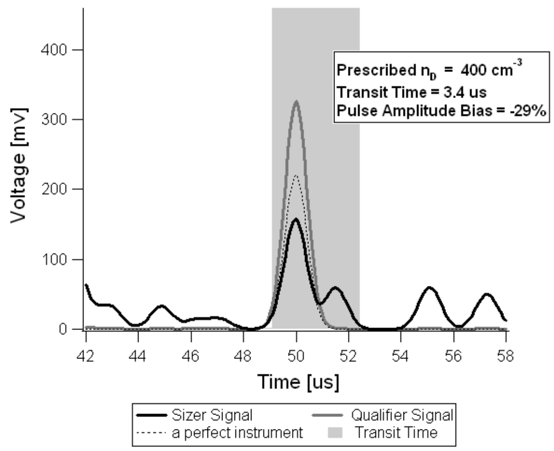
Prescribed $n_D$ = 400 $cm^{-3}$
Transit Time = 3.4 us
Pulse Amplitude Bias = -29%
Voltage [mv]
Time [us]
Sizer Signal
Qualifier Signal
a perfect instrument
Transit Time

**(a)**

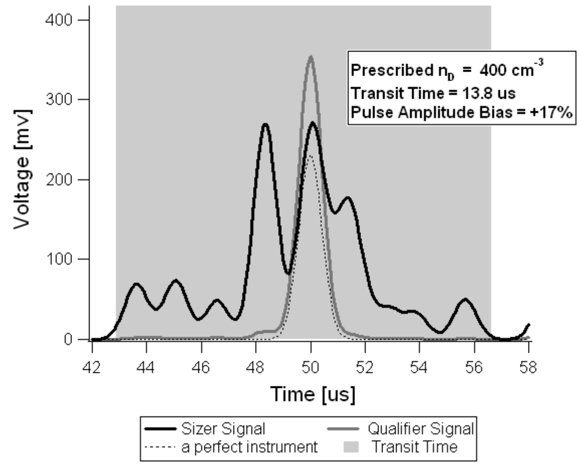
Prescribed $n_D$ = 400 $cm^{-3}$
Transit Time = 13.8 us
Pulse Amplitude Bias = +17%
Voltage [mv]
Time [us]
Sizer Signal
Qualifier Signal
a perfect instrument
Transit Time

**(b)**

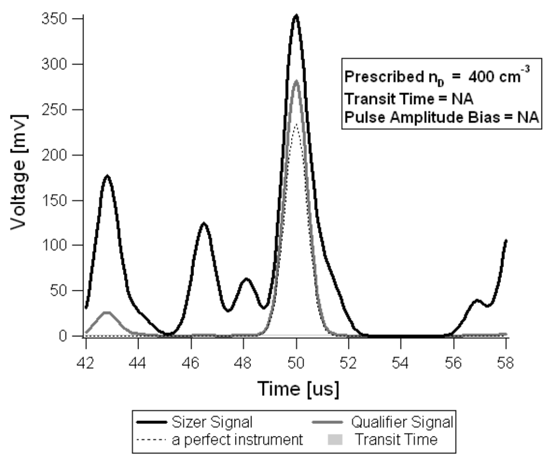
Prescribed $n_D$ = 400 $cm^{-3}$
Transit Time = NA
Pulse Amplitude Bias = NA
Voltage [mv]
Time [us]
Sizer Signal
Qualifier Signal
a perfect instrument
Transit Time

**(c)**

**Figure 8.**

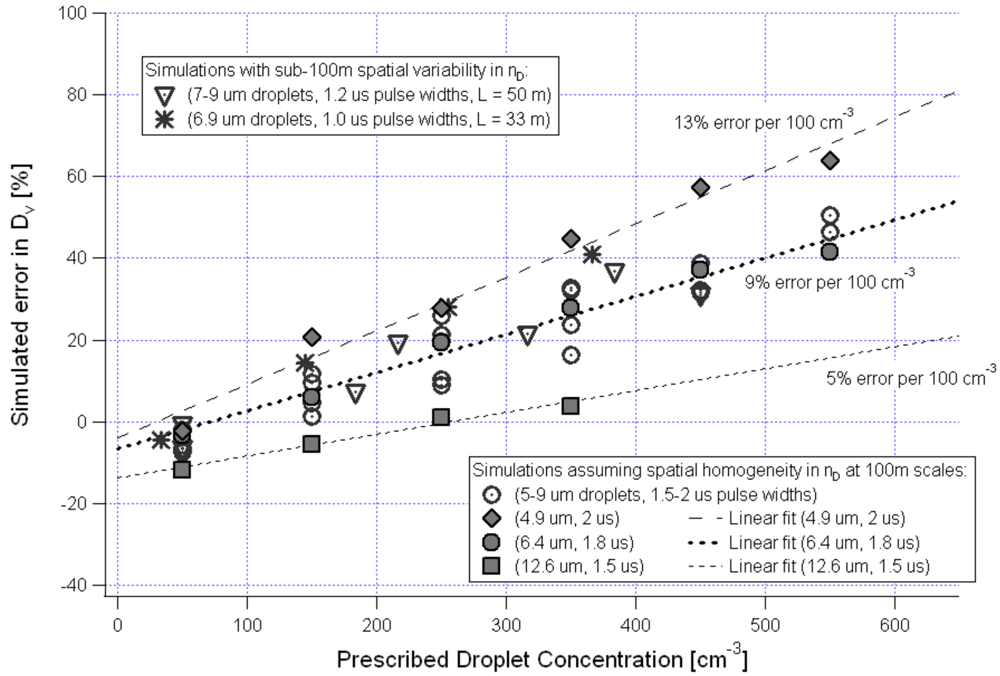

Simulations with sub-100m spatial variability in $n_D$:
(7-9 um droplets, 1.2 us pulse widths, L = 50 m)
(6.9 um droplets, 1.0 us pulse widths, L = 33 m)
13% error per 100 cm$^{-3}$
9% error per 100 cm$^{-3}$
5% error per 100 cm$^{-3}$
Simulations assuming spatial homogeneity in $n_D$ at 100m scales:
(5-9 um droplets, 1.5-2 us pulse widths)
(4.9 um, 2 us)
(6.4 um, 1.8 us)
(12.6 um, 1.5 us)
Linear fit (4.9 um, 2 us)
Linear fit (6.4 um, 1.8 us)
Linear fit (12.6 um, 1.5 us)
Simulated error in $D_v$ [%]
Prescribed Droplet Concentration [cm$^{-3}$]


**(a)**

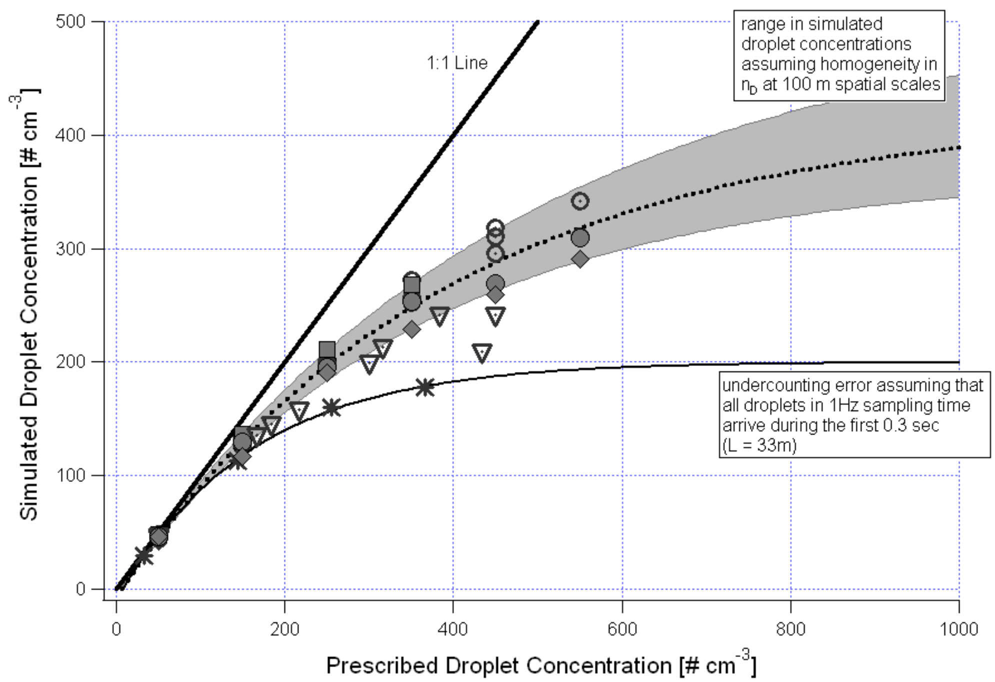

1:1 Line
range in simulated droplet concentrations assuming homogeneity in $n_D$ at 100 m spatial scales
undercounting error assuming that all droplets in 1Hz sampling time arrive during the first 0.3 sec (L = 33m)
Simulated Droplet Concentration [# cm$^{-3}$]
Prescribed Droplet Concentration [# cm$^{-3}$]


**(b)**

**Figure 9.**

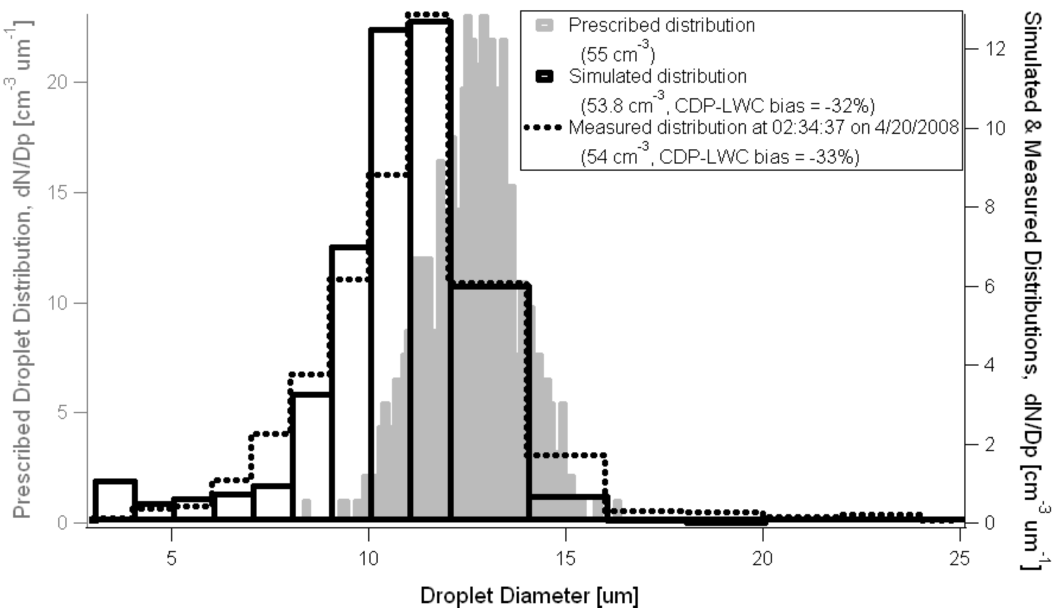

Prescribed distribution
(55 cm$^{-3}$)
Simulated distribution
(53.8 cm$^{-3}$, CDP-LWC bias = -32%)
Measured distribution at 02:34:37 on 4/20/2008
(54 cm$^{-3}$, CDP-LWC bias = -33%)
Prescribed Droplet Distribution, dN/Dp [cm$^{-3}$ um$^{-1}$]
Simulated & Measured Distributions, dN/Dp [cm$^{-3}$ um$^{-1}$]
Droplet Diameter [um]


**(a)**

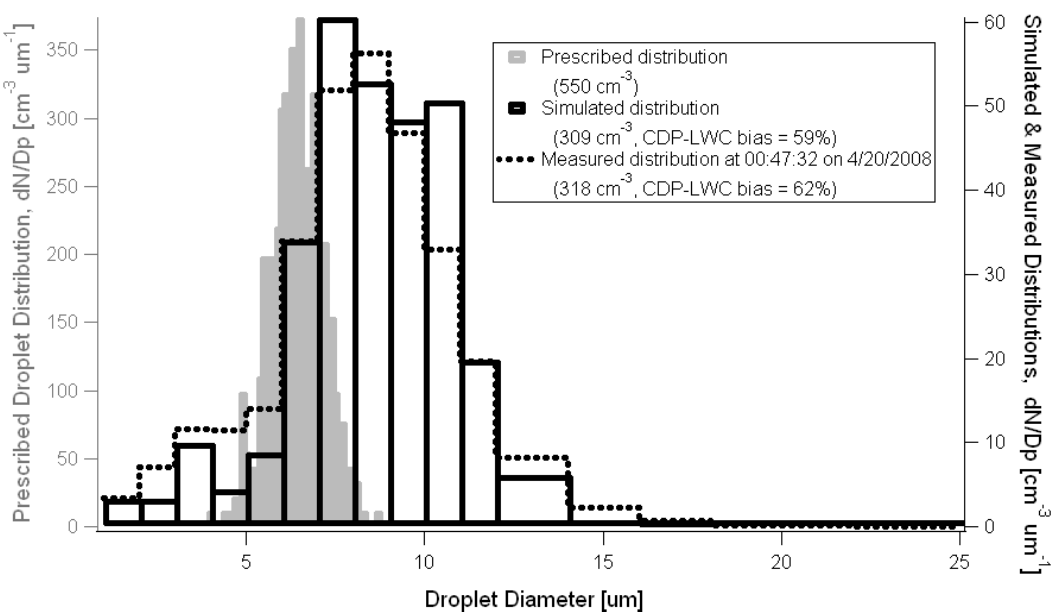

Prescribed distribution
(550 cm$^{-3}$)
Simulated distribution
(309 cm$^{-3}$, CDP-LWC bias = 59%)
Measured distribution at 00:47:32 on 4/20/2008
(318 cm$^{-3}$, CDP-LWC bias = 62%)
Prescribed Droplet Distribution, dN/Dp [cm$^{-3}$ um$^{-1}$]
Simulated & Measured Distributions, dN/Dp [cm$^{-3}$ um$^{-1}$]
Droplet Diameter [um]


**(b)**

**Figure 10.**

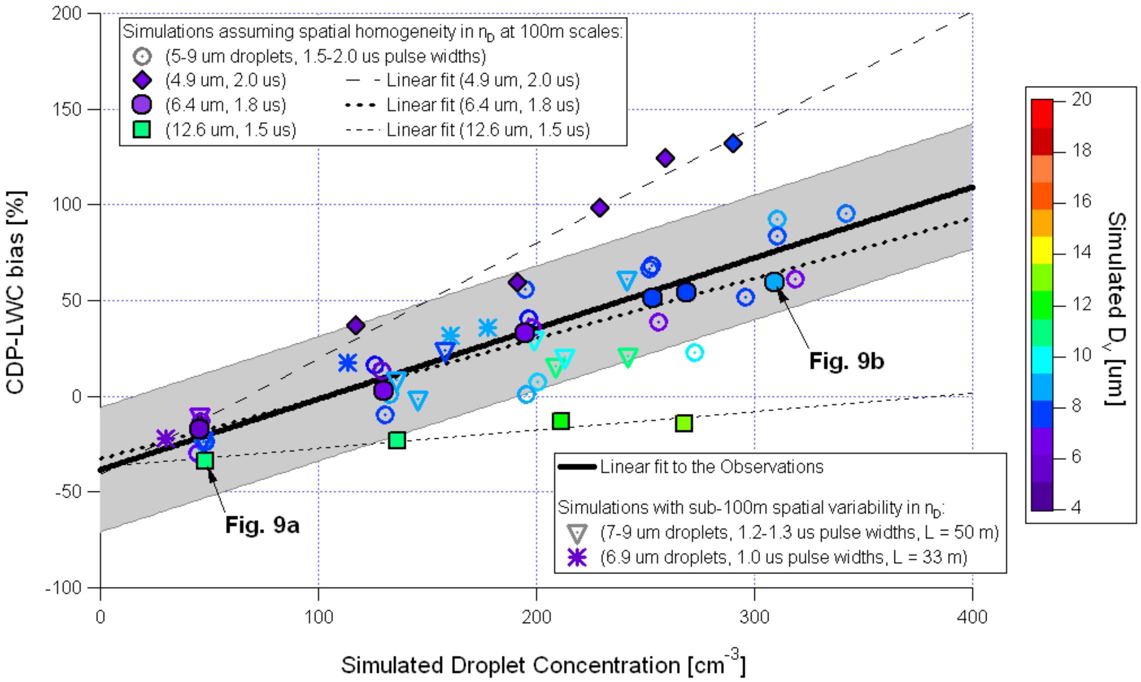

Simulations assuming spatial homogeneity in $n_D$ at 100m scales:
(5-9 um droplets, 1.5-2.0 us pulse widths)
(4.9 um, 2.0 us)
(6.4 um, 1.8 us)
(12.6 um, 1.5 us)
Linear fit (4.9 um, 2.0 us)
Linear fit (6.4 um, 1.8 us)
Linear fit (12.6 um, 1.5 us)
Linear fit to the Observations
Simulations with sub-100m spatial variability in $n_D$:
(7-9 um droplets, 1.2-1.3 us pulse widths, L = 50 m)
(6.9 um droplets, 1.0 us pulse widths, L = 33 m)
Fig. 9a
Fig. 9b
CDP-LWC bias [%]
Simulated Droplet Concentration [cm$^{-3}$]
Simulated $D_v$ [um]
200
150
100
50
0
-50
-100
0
100
200
300
400
20
18
16
14
12
10
8
6
4

**Figure 11.**

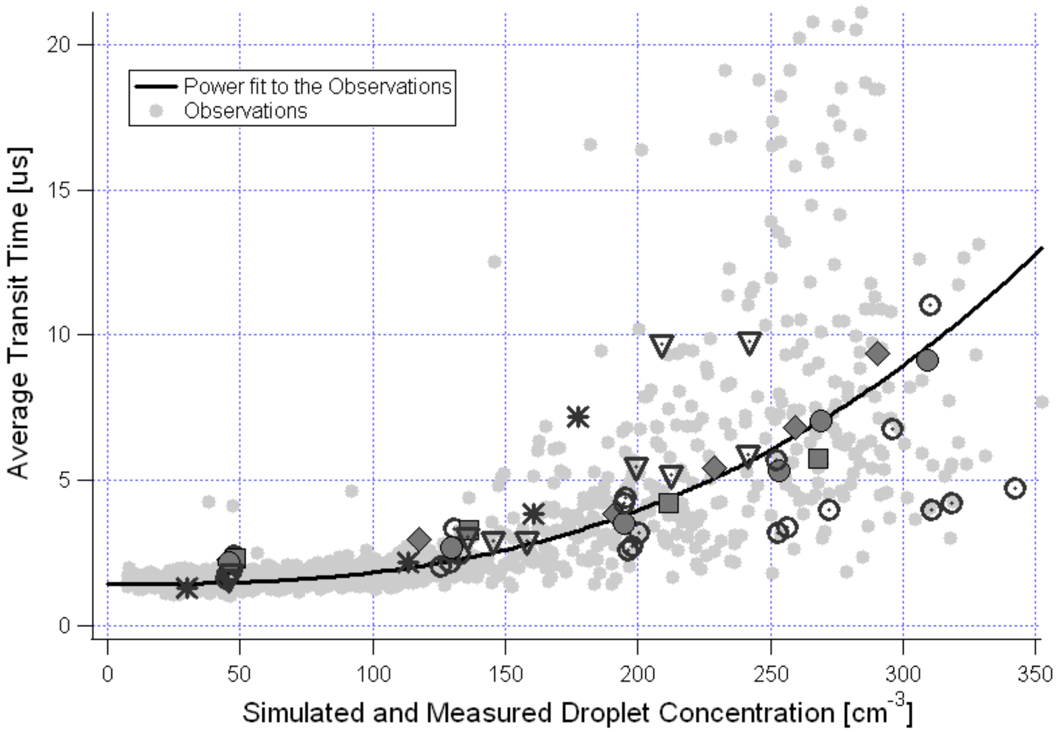
Power fit to the Observations
Observations
Average Transit Time [us]
Simulated and Measured Droplet Concentration [cm$^{-3}$]
0
5
10
15
20
0
50
100
150
200
250
300
350